https://doi.org/10.5194/essd-2019-126
Preprint. Discussion started: 7 August 2019


Open Access Earth System Science Data Discussions

# Improved estimate of global gross primary production for reproducing its long-term variation, 1982-2017

Yi Zheng[1], Ruoque Shen[1], Yawen Wang[1,2], Xiangqian Li[1], Shuguang Liu[3], Shunlin Liang[4,5], Jing M. Chen[6,7], Weimin Ju[7,8], Li Zhang[9], Wenping Yuan[1,2*]

[1]School of Atmospheric Sciences, Sun Yat-sen University, Guangzhou 510245, Guangdong, China;
[2]Southern Laboratory of Ocean Science and Engineering (Guangdong, Zhuhai), Zhuhai 519000, Guangdong, China
[3]College of Life Science and Technology, Central South University of Forestry and Technology (CSUFT), Changsha, Hunan 410004, China
[4]Department of Geographical Sciences, University of Maryland, College Park, MD 20742 USA
[5]School of Remote Sensing Information Engineering, Wuhan University, Wuhan 430072, Hubei, China
[6]Department of Geography, University of Toronto, Canada, M5G 3G3
[7]International Institute for Earth System Sciences, Nanjing University, Nanjing, China.
[8]Jiangsu Center for Collaborative Innovation in Geographical Information Resource Development and Application, Nanjing, China.
[9]Key Laboratory of Digital Earth Science, Institute of Remote Sensing and Digital Earth, Chinese Academy of Sciences, Beijing 100094, China

*Correspondence to*: yuanwpcn@126.com (W. Yuan).

**Abstract.** Satellite-based models have been widely used to simulate vegetation gross primary production (GPP) at site, regional, or global scales in recent years. However, accurately reproducing the interannual variations in GPP remains a major challenge, and the long-term changes in GPP remain highly uncertain. In this study, we generated a long-term global GPP dataset at 0.05 ° latitude by 0.05 ° longitude at 8-day interval by revising a light use efficiency model (i.e. EC-LUE). In the revised EC-LUE model, we integrated the regulations of several major environmental variables: atmospheric $CO_2$ concentration, radiation components, and atmospheric vapor pressure deficit (VPD). These environmental variables showed substantial long-term changes, which could greatly impact the global vegetation productivity. Eddy covariance (EC) measurements at 84 towers from the FLUXNET2015 dataset, covering nine major ecosystem types of the globe, were used to calibrate and validate the model. The revised EC-LUE model could explain 83% and 68% of the spatial variations in the annual GPP at 42 calibration and 43 validation sites, respectively. In particular, the revised EC-LUE model could very well reproduce (~74% sites $R^2$ >0.5; averaged $R^2$ = 0.65) the interannual variations in GPP at 51 sites with observations greater than 5-years. At global scale, sensitivity analysis indicated that the long-term changes of environmental variables could be well reflected in the global GPP dataset. The $CO_2$ fertilization effect on the global GPP (0.14 ± 0.001 Pg C $yr^{-1}$) could be offset by the increased VPD (−0.16 ± 0.02 Pg C $yr^{-1}$). The global GPP derived from different datasets exist substantial uncertainty in magnitude and interannual variations. The magnitude of global summed GPP simulated by the revised EC-LUE model was comparable to other global models. While the revised EC-LUE model has a unique superiority in simulating the interannual variations in GPP at both site level and global scales. The revised EC-LUE model provides a reliable long-

https://doi.org/10.5194/essd-2019-126
Preprint. Discussion started: 7 August 2019


Open Access Earth System Science Data Discussions

term estimate of global GPP because of integrating the important environmental variables. The dataset is available at https://doi.org/10.6084/m9.figshare.8942336 (Zheng et al., 2019).

## 1 Introduction

Vegetation gross primary production (GPP) is the largest carbon flux component within terrestrial ecosystems and plays an essential role in regulating the global carbon cycle (Canadell et al., 2007; Zhao et al., 2010). As a primary variable of the terrestrial ecosystem cycle, GPP estimates will substantially determine other variables of the carbon cycle (Yuan et al., 2011). Satellite-based GPP models have been developed based on the light use efficiency (LUE) principle (Monteith, 1972; Potter et al., 1993; Running et al., 2004; Xiao et al., 2005; Yuan et al., 2007). Thus far, LUE models have been a major tool for investigating the spatio-temporal changes in GPP and the environmental dominates, either independently or by combining with other ecosystem models (Keenan et al., 2016; Smith et al., 2016).

However, current LUE models exhibit a poor performance in reproducing the interannual variations in GPP. A previous study indicated that seven LUE models only could explain 6–36% of the interannual variations in GPP at 51 eddy covariance (EC) towers (Yuan et al., 2014). Similarly, a model comparison showed that none of the examined 16 biophysical models nor the 3 satellite-based models could consistently reproduce the observed interannual variations in carbon exchange at 11 forest sites in North America (Keenan et al., 2012). Seven LUE models simulated the long-term trends of global GPP varied from −0.15 to 1.09 Pg C $yr^{-1}$ (Cai et al., 2014). An important reason for the poor performance in modeling the interannual variability is that the effect of environmental regulations on vegetation production is not completely integrated in the LUE models (Stocker et al., 2019). In particular, the long-term changes in several environmental variables are very important for accurately simulating the GPP series at the decadal scale.

Several environmental variables should be included in GPP models. Firstly, as we all know the rising atmospheric $CO_2$ concentration in the past few decades substantially stimulated global vegetation growth (Zhu et al., 2016; Liu et al., 2017). Field experiments using greenhouses or open-top chambers showed that an increase of approximate 300 ppm in $CO_2$ concentration can increase C3 plant photosynthesis on the order of 60% (Norby et al., 1999). Free-air $CO_2$ enrichment (FACE) experiments generally confirmed the enhancement in net primary production (NPP) with the rising $CO_2$ concentration (Ainsworth and Long, 2005). For example, four FACE experiments indicated that the forest NPP consistently increased at the median of 23 ± 2% when the ambient $CO_2$ concentration was elevated to approximately 550 ppm (Norby et al., 2005). According to observations, the atmospheric $CO_2$ concentration has risen by approximately 20% from 340 ppm (1982) to 410 ppm (2018) (https://www.esrl.noaa.gov/). However, the effects of $CO_2$ fertilization on GPP have not been integrated in most current satellite-based LUE models.

Secondly, solar radiation, or more specifically the photosynthetic active radiation (PAR) substantially influences the vegetation production of terrestrial ecosystem (Alton et al., 2007; Kanniah et al., 2012; Krupkova et al., 2017). Study indicated that the solar radiation incident at the earth surface underwent significant decadal variations (Wild et al., 2005). A

https://doi.org/10.5194/essd-2019-126
Preprint. Discussion started: 7 August 2019




comprehensive analysis based on the datasets of worldwide distributed sites indicated significant decreases in solar radiation (2% per decade) from the late 1950s to 1990 in the regions of Asia, Europe, North America, and Africa (Gilgen et al., 1998). A later assessment by Wild et al. (2005) showed that the radiation increased at widespread locations since the mid-1980s.

However, it is not only the total amount of solar radiation or PAR incident at the surface, but also, more importantly, their partitioning into direct and diffuse radiations, that impact the vegetation productivity (Urban et al., 2007; Kanniah et al., 2012). Increased proportion of diffuse radiation enhances vegetation photosynthesis, because a higher blue/red light ratio within the diffuse radiation may lead to higher light use efficiency (Gu et al., 2002; Alton et al., 2007). For example, the sharply increased diffuse radiation induced by the 1991 Mount Pinatubo eruption enhanced the noontime vegetation productivity of a deciduous forest in the next 2 years (Gu et al. 2003). Besides volcanic aerosols, clouds could also reduce the total and direct radiation, while increase the proportion of diffuse radiation. Yuan et al. (2010) found that the higher LUE at European forests than North America was because of the higher ratio of cloudy days in Europe. Yuan et al. (2014) further proved that the significantly underestimated GPP during cloudy days by six LUE models was because the effects of diffuse radiation on LUE were neglected in these models.

Thirdly, atmospheric vapor pressure deficit (VPD) is another factor that should be included in GPP models. As an important driver of atmospheric water demand for plants, VPD influences terrestrial ecosystem function and photosynthesis (Rawson et al., 1977). Rising air temperature increases the saturated vapor pressure at a rate of ~7%/K according to the Classius–Clapeyron relationship, and therefore, VPD will increase if the atmospheric water vapor content does not increase by exactly the amount of saturated vapor pressure. Numerous studies indicated significant changes in the relative humidity (ratio of actual water vapor pressure to saturated water vapor pressure) in both humid areas and continental areas located far from oceanic humidity (Van Wijngaarden and Vincent, 2004; Pierce et al., 2013). In particular, the global averaged land surface relative humidity decreased sharply after the late 1990s (Simmons et al. 2010; Willett et al. 2014). The leaf and canopy photosynthetic rate decline when the atmospheric VPD increases due to stomatal closure (Fletcher et al., 2007). A recent study highlighted that increases in VPD rather than changes in precipitation will be a dominant influence on vegetation productivity (Konings et al., 2017). However, the influence of long-term VPD variations is not well expressed in many LUE models currently.

We have developed a LUE model, namely the EC-LUE model, by integrating remote sensing data and eddy covariance data to simulate daily GPP (Yuan et al., 2007; 2010). The model has been evaluated using the observations at EC towers located in Europe, North America, China, and East Asia, covering various ecosystem types (Yuan et al., 2007; 2010; Li et al., 2013). In this study, we revised the EC-LUE model by integrating the impacts of several environmental variables (i.e., atmospheric $CO_2$ concentration, radiation components, and atmospheric VPD) across a long-term temporal scale. Firstly, we evaluated the effectiveness of the revised EC-LUE model in determining the spatial, seasonal, and interannual variations in GPP from multiple eddy covariance sites. Then, a global GPP dataset at 0.05 ° spatial resolution was generated. Finally, we analyzed the contributions of the aforementioned environmental variables to the global GPP and discussed the spatial and interannual variations in different global GPP datasets.

https://doi.org/10.5194/essd-2019-126
Preprint. Discussion started: 7 August 2019


Open Access Earth System Science Data Discussions

## 2 Data and Methods

### 2.1 Description of the revised EC-LUE model

The terrestrial vegetation GPP can be expressed as follows in the revised EC-LUE model:

$$GPP = (\varepsilon_{msu} \times APAR_{su} + \varepsilon_{msh} \times APAR_{sh}) \times C_s \times \min(T_s, W_s) \quad (1)$$

where $\varepsilon_{msu}$ is the maximum LUE of sunlit leaves; $APAR_{su}$ is the PAR absorbed by sunlit leaves; $\varepsilon_{msh}$ is the maximum LUE of shaded leaves; $APAR_{sh}$ is the PAR absorbed by shaded leaves; $C_s$, $T_s$, and $W_s$ represent the downward regulation scalars of atmospheric $CO_2$ concentration ([$CO_2$]), air temperature, and VPD on LUE ranging from 0 to 1; *min* represents the minimum value.

The effect of atmospheric $CO_2$ concentration on GPP is determined by the following equations (Farquhar et al., 1980; Collatz et al., 1991):

$$C_s = \frac{C_i - \varphi}{C_i + 2\varphi} \quad (2)$$

$$C_i = C_a \times \chi \quad (3)$$

where $\varphi$ is the $CO_2$ compensation point in the absence of dark respiration (ppm); $C_i$ is the leaf internal $CO_2$ concentration; $C_a$ is the atmospheric $CO_2$ concentration; $\chi$ is the ratio of leaf internal to atmospheric $CO_2$ which can be estimated as follows (Prentice et al., 2014; Keenan et al., 2016):

$$\chi = \frac{\varepsilon}{\varepsilon + \sqrt{VPD}} \quad (4)$$

$$\varepsilon = \sqrt{\frac{356.51K}{1.6\eta^*}} \quad (5)$$

$$K = K_c\left(1 + \frac{P_0}{K_0}\right) \quad (6)$$

$$K_c = 39.97 \times e^{\frac{79.43 \times (T - 298.15)}{298.15RT}} \quad (7)$$

$$K_o = 27480 \times e^{\frac{36.38 \times (T - 298.15)}{298.15RT}} \quad (8)$$

where $K_c$ and $K_o$ are the Michaelis–Menten constants for $CO_2$ and $O_2$; $P_o$ is the partial pressure of $O_2$; *Ta* is air temperature (K); $\eta^*$ is the viscosity of water relative to its value at 25 ℃ depending on the air temperature (Korson et al., 1969); *R* is the molar gas constant (8.314 J $mol^{-1}$ $K^{-1}$).

$T_s$ and $W_s$ can be expressed as follows:

$$T_s = \frac{(T - T_{min}) \times (T - T_{max})}{(T - T_{min}) \times (T - T_{max}) - (T - T_{opt}) \times (T - T_{opt})} \quad (9)$$

$$W_s = \frac{VPD_0}{VPD_0 + VPD} \quad (10)$$

where $T_{min}$, $T_{opt}$, and $T_{max}$ are the minimum, optimum, and maximum temperatures (K) for vegetation photosynthesis, respectively (Yuan et al., 2007); $VPD_0$ is the half saturation coefficient of the VPD constraint equation (kPa).

$APAR_{su}$ and $APAR_{sh}$ can be expressed as follows (Chen et al., 1999):

https://doi.org/10.5194/essd-2019-126
Preprint. Discussion started: 7 August 2019


Open Access Earth System Science Data Discussions

$$APAR_{su} = (PAR_{dir} \times \frac{\cos(\beta)}{\cos(\theta)} + \frac{PAR_{dif} - PAR_{dif,u}}{LAI} + C) \times LAI_{su} \quad (11)$$

$$APAR_{sh} = (\frac{PAR_{dif} - PAR_{dif,u}}{LAI} + C) \times LAI_{sh} \quad (12)$$

$$PAR_{dif,u} = PAR_{dif} \times \exp(\frac{-0.5 \times \Omega \times LAI}{\cos(\bar{\theta})}) \quad (13)$$

where $PAR_{dir}$ is the direct PAR; $PAR_{dif}$ is the diffuse PAR; $PAR_{dif,u}$ is the diffuse PAR under the canopy; C represents the multiple scattering effects of direct radiation; $\Omega$ is the clumping index, which is set according to vegetation types (Tang et al., 2007); $\theta$ is the solar zenith angle; $\beta$ is the mean leaf–sun angle, which is set to 60 °; $\bar{\theta}$ is the representative zenith angle for diffuse radiation transmission and can be expressed by LAI (Chen et al., 1999):

$$\cos(\bar{\theta}) = 0.537 + 0.025 \times LAI \quad (14)$$

The LAIs of shaded leaves ($LAI_{sh}$) and sunlit leaves ($LAI_{su}$) in Eqs. (11) and (12) are computed following Chen et al (1999):

$$LAI_{su} = 2 \times \cos(\theta) \times \left(1 - e^{-0.5 \times \Omega \times \frac{LAI}{\cos(\theta)}}\right) \quad (15)$$

$$LAI_{sh} = LAI - LAI_{su} \quad (16)$$

The parameters $\varepsilon_{msu}$, $\varepsilon_{msh}$, $\varphi$, and $VPD_0$ were calibrated using the estimated GPP from EC towers. The initial ranges of $\varepsilon_{msu}$ and $\varepsilon_{msh}$ were set to 0–12 g C $MJ^{-1}$, $\varphi$ was set to 0–100 ppm, $VPD_0$ was set to 0–4 kPa. The optimized values of these parameters were adopted until the root mean square error (RMSE) of the model simulated and the EC estimated daily GPP approached to the minimum value.

### 2.2 Data from the eddy covariance towers

The FLUXNET2015 dataset (http://www.fluxdata.org) includes over 200 variables of carbon fluxes, energy fluxes, and meteorological data collected and processed at sites by the FLUXNET community. In our study, eighty-four EC sites in FLUXNET2015 dataset were utilized to optimize the parameters and evaluate the performance of the revised EC-LUE model, including nine major terrestrial ecosystem vegetation types (Table 1): evergreen broadleaf forests (EBF), evergreen needleleaf forests (ENF), deciduous broadleaf forests (DBF), mixed forests (MF), grasslands (GRA), savannas (SAV), shrubland (SHR), wetlands (WET), and croplands (CRO). More information about the characteristics of these sites can be referred to the FLUXNET website. For each site, the aggregated daily GPP, PAR, air temperature (Ta), and VPD were used in our study. The daily meteorological variables were gap-filled and/or downscaled from the ERA-interim reanalysis dataset in both space and time (Vuichard and Papale, 2015). The carbon flux measurements (i.e., net ecosystem exchange (NEE)) were gap-filled and partitioned into GPP and ecosystem respiration (Re) using a nighttime based approach (Reichstein et al. 2005). The gap-filled technique of the carbon flux measurements and meteorological variables is the marginal distribution sampling (MDS) method described in Reichstein et al. (2005).

<<Table 1>>

https://doi.org/10.5194/essd-2019-126
Preprint. Discussion started: 7 August 2019


Open Access Earth System Science Data Discussions

### 2.3 Data at the global scale

The input data of the revised EC-LUE model are shown in Table2. The global scale meteorological reanalysis dataset was derived from the second Modern-Era Retrospective analysis for Research and Applications (MERRA-2) dataset. It was produced by NASA's Global Modeling and Assimilation Office that uses an upgraded version of the GEOS-5 (Rienecker et al., 2011). It has been validated carefully using surface meteorological datasets and enhanced assimilation system to reduce the uncertainty in various meteorological variables globally. In our study, we obtained the daily air temperature ($T_a$, ℃), dew point temperature ($T_d$, ℃), direct PAR, and diffuse PAR at 0.625 ° in longitude by 0.5 ° in latitude from 1982 to 2017. VPD was calculated from air temperature and dew point temperature:

$$SVP = 6.112 \times e^{\frac{17.67T_a}{T_a+243.5}} \quad (17)$$

$$RH = e^{\frac{17.625T_d}{T_d+243.04}-\frac{17.625T_a}{T_a+243.04}} \quad (18)$$

$$VPD = SVP \times (1 - RH) \quad (19)$$

where SVP is the saturated vapor pressure (k Pa), and RH is the relative humidity.

The 8-day Global LAnd Surface Satellite-leaf area index (GLASS LAI) dataset at 0.05 ° latitude by 0.05 ° longitude was adopted to indicate vegetation growth from 1982 to 2017. It was produced using the general regression neural networks (GRNNs) trained with the fused MOD15 LAI and CYCLOPES LAI and the preprocessed MODIS/AVHRR reflectance data over the BELMANIP sites (Xiao et al., 2016). Products validation and comparison showed that the GLASS LAI product was spatially complete and temporally continuous with lower uncertainty (Xu et al., 2018).

Additionally, the MCD12Q1 product with IGBP classification scheme was used as land cover map and the NOAA's Earth System Research Laboratory (ESRL) $CO_2$ concentration dataset was used to express the $CO_2$ fertilization effect.

<<Table 2>>

### 2.4 Environmental contributions to long-term changes in GPP

To evaluate the contribution of the major environmental variables to GPP, including the atmospheric $CO_2$ concentration ([$CO_2$]), climate, and satellite-based LAI, two types of experimental simulations where performed. The first simulation experiment ($S_{ALL}$) was a normal model run, with all the environmental drivers changing over time. In the second type of simulation experiments ($S_{CLI0}$, $S_{LAI0}$, and $S_{CO20}$), two driving factors could be varied with time while maintaining the third constant at an initial baseline level. For example, the $S_{CLI0}$ simulation experiment allowed the LAI and atmospheric [$CO_2$] to vary with time while the climate variables were kept constant at 1982 values. The $S_{LAI0}$ and $S_{CO20}$ simulation experiments kept LAI and atmospheric [$CO_2$] constant at 1982 values and varied the other two variables.

Considering the differences between the simulation results of the first type ($S_{ALL}$) and second type ($S_{CO20}$ and $S_{LAI0}$) of experiments, the GPP sensitivities to atmospheric [$CO_2$] ($\beta_{CO2}$) and LAI ($\beta_{LAI}$) were estimated as follows:

$$\Delta GPP_{(S_{ALL}-S_{CO20})i} = \beta_{CO2} \times \Delta CO2_{(S_{ALL}-S_{CO20})i} + \varepsilon \quad (20)$$

https://doi.org/10.5194/essd-2019-126
Preprint. Discussion started: 7 August 2019




$$\Delta GPP_{(S_{ALL}-S_{LAI0})i} = \beta_{LAI} \times \Delta LAI_{(S_{ALL}-S_{LAI0})i} + \varepsilon \quad (21)$$

where $\Delta GPP_i$, $\Delta CO2_i$, and $\Delta LAI_i$ denote the differences in the GPP simulations, atmospheric [$CO_2$], and *LAI* between the two model experiments from 1982 to 2017, and ε is the stochastic error term.

The GPP sensitivities to the three climate variables: air temperature ($\beta_{Ta}$), VPD ($\beta_{VPD}$), and PAR ($\beta_{PAR}$) were calculated using a multiple regression approach:

$$\Delta GPP_{(S_{ALL}-S_{CLI0})i} = \beta_{Ta} \times \Delta Ta_{(S_{ALL}-S_{CLI0})i} + \beta_{VPD} \times \Delta VPD_{(S_{ALL}-S_{CLI0})i} + \beta_{PAR} \times \Delta PAR_{(S_{ALL}-S_{CLI0})i} + \varepsilon \quad (22)$$

where $\Delta Ta_i$, $\Delta VPD_i$, and $\Delta PAR_i$ denote the differences in Ta, VPD, and PAR time series between the two model experiments ($S_{ALL}$ and $S_{CLI0}$), respectively. The regression coefficient $\beta$ was estimated using the maximum likelihood analysis.

### 2.5 Statistical analysis

Coefficient of determination ($R^2$), RMSE, and bias (the difference between observations and simulations) were adopted to evaluate the performance of the revised EC-LUE model.

## 3 Results

### 3.1 Parameter optimization and model validation

This study used EC measurements at 42 sites to calibrate the parameter values and 43 sites to validate the model accuracy of the revised EC-LUE model. The parameters ($\varepsilon_{msu}$, $\varepsilon_{msh}$, φ, and $VPD_0$) of each vegetation type are shown in Table 3. We evaluated the model performance by using the tower-derived meteorology data and global reanalysis meteorology, respectively. In general, the revised EC-LUE model could effectively reproducing the spatial, seasonal, and annual variations in the tower-estimated GPP at most of the calibration and validation sites (Figs. 1–4).

<< Table 3>>

By using the tower-derived meteorology data, the revised EC-LUE model explained 76% of the spatial variations in GPP across all the calibration and validation sites with no obvious systematic errors (Fig. 1(a)). Furthermore, the model respectively explained 83% and 67% of the spatial variations in GPP at the calibration and validation sites. In contrast, the model performance decreased when using the meteorological reanalysis dataset, explaining only 52% of the spatial variations in the GPP and slightly overestimating the GPP at the sites with low/moderate GPP values (Fig. 1(b)).

<<Figure 1>>

Similarly, the revised EC-LUE model also shows a good performance in reproducing the seasonal variations in the GPP at most EC sites (Figs. 2–3). By using the tower-derived meteorology data, the averaged $R^2$ over the calibration and validation sites was 0.78 and 0.72, respectively. Over 92% of the calibration and validation sites showed high $R^2$ (>0.5). The two low $R^2$ (< 0.4) sites (i.e., BR-Sa1 and BR-Sa3) were tropical forests without pronounced seasonal pattern of GPP (Fig. 2(a); Fig. 3(a)). The RMSE and the absolute value of bias varied from 0.68 (CN-Du2) to 5.72 (US-Ne1) g C $m^{-2}$ $d^{-1}$ and from 0.002

https://doi.org/10.5194/essd-2019-126
Preprint. Discussion started: 7 August 2019




(CA-NS1) to 2.12 (US-ARM) g C $m^{-2}$ $d^{-1}$, respectively. The averaged RMSE and the absolute value of bias over all the sites were 2.64 and 0.67 g C $m^{-2}$ $d^{-1}$, respectively (Fig. 2(b)–(c); Fig. 3(b)–(c)). Additionally, there is no obvious difference between the seasonal GPP performance when using the tower-derived meteorology data and meteorological reanalysis dataset (Figs. 2–3).

<<Figure 2/ Figure 3>>

The ability of the LUE models to reproduce the interannual variations in GPP was investigated at 51 EC towers with observations greater than 5-years (Table 1; Fig. 4). We examined the relations between the mean annual GPP simulations and observations at each site and used the coefficient correlation ($R^2$) and slope of the regression relationship to investigate the model capability in simulating the interannual variations in GPP. The result showed that the revised EC-LUE model could effectively determine the interannual variations in GPP (Fig. 4). Approximately 74% of the sites showed higher $R^2$ values (>0.5) for both tower-derived meteorology and reanalysis meteorology derived models (Fig. 4(a)). The mean values of $R^2$ between the revised EC-LUE model simulated GPP and the tower estimated GPP were 0.65 and 0.61 for the models derived from tower-derived meteorology and reanalysis meteorology, and both the $R^2$ values are higher than the original EC-LUE model (0.36) and other LUE models (<0.30) (Fig. 4(c)). The averaged slopes of the revised EC-LUE model were 0.71 and 0.64 for tower-derived meteorology and reanalysis meteorology derived models, while the slope of the original EC-LUE model was 0.56 (Fig. 4(c)).

<<Figure 4>>

### 3.2 Spatio-temporal patterns of global GPP

A global GPP dataset at 0.05 °latitude by 0.05 °longitude was generated ranging from 1982 to 2017 based on the revised EC-LUE model. The long-term averaged value of the global summed GPP was 125.3 ± 3.13 Pg C $yr^{-1}$ across the vegetated area. Fig. 5 shows the global distributed patterns of the annual averaged GPP for each pixel. The GPP was high over the tropical forest areas, such as Amazon and Southeast Asia, where the moisture and temperature conditions are sufficient for photosynthesis (Fig. 5(a)). The GPP decreased with the decreasing gradients of temperature and precipitation (Fig. 5(b)). The temperate and subhumid regions have moderate GPP; and the lowest GPP is located in arid or cold regions, where either precipitation or temperature is limited (Fig. 5(b)).

<<Figure 5>>

GPP trends over the period of 1982–2017 were determined for each pixel using a linear regression analysis (Fig. 6). In general, the revised EC-LUE model predicted an increased trend in the annual mean GPP from 1982 to 2017. Approximately 69.5% of the vegetated areas, mainly located in temperate and humid regions, showed increased trends. The spatial distributed patterns of GPP trend along with the temperature and precipitation gradients was more heterogeneous than that of the mean annual GPP (Fig. 5(b); Fig. 6(b)). The decreased GPP areas were mainly distributed in the tropic regions with abundant precipitation and high temperature, particularly in the Amazon forest. The cold or arid areas exhibited less variations in GPP (Fig. 6(b)).

https://doi.org/10.5194/essd-2019-126
Preprint. Discussion started: 7 August 2019




<<Figure 6>>

### 3.3 Contributions of environmental variables to GPP

To quantify the contributions of the environmental variables to long-term changes in GPP, we explored the sensitivity of global summed GPP to climate variables (i.e., VPD, Ta, and PAR), LAI, and atmospheric $CO_2$ (Fig. 7). The global summed GPP generated from different experimental simulations (section 2.4) exhibited differently in terms of the annual mean value, trend, and standard deviation (Fig. 7(a)). The normal simulated GPP ($S_{ALL}$ GPP, all the environmental drivers changing over time) significantly increased at the rate of 0.17 Pg C $yr^{-1}$, while the increasing rate of $S_{CLI0}$ GPP (climate variables were kept constant at 1982 values) was even greater (0.36 Pg C $yr^{-1}$). On the contrary, the $S_{LAI0}$ GPP (LAI was kept constant at 1982 values) showed a significantly decreasing trend (−0.06 Pg C $yr^{-1}$), and the $S_{CO20}$ GPP (atmospheric [$CO_2$] was kept constant at 1982 values) showed an insignificantly increasing trend (Fig. 7(a)). The sensitivity analysis showed that the global GPP decreased by approximately 6 Pg C with a 0.1 kPa increase in VPD. This is comparable to the increase in GPP with a 100 ppm rise in atmospheric [$CO_2$] (i.e., $\beta_{CO2}$ = 7.62 ± 0.04 Pg C 100 $ppm^{-1}$) or 0.1 unit greening of LAI (i.e., $\beta_{LAI}$ = 5.98 ± 0.09 Pg C 0.1 $unit^{-1}$) or 100 MJ increase in PAR (i.e., $\beta_{PAR}$ = 5.76 ± 0.23 Pg C 100 $MJ^{-1}$) (Fig. 7(b)). Over the period of 1982–2017, the increased VPD resulted in the global GPP decreases of −0.16 ± 0.02 Pg C $yr^{-1}$, which offset the fertilization effect of $CO_2$ (0.14 ± 0.001 Pg C $yr^{-1}$). The global GPP showed a decreased trend after 2001 due to the joint effect of increased VPD and decreased PAR (Fig. 7(c)). While the increased trend of GPP before 2000 was mainly affected the increased PAR and greening of LAI (Fig. 7(c)).

<<Figure 7>>

## 4 Discussion

### 4.1 Model accuracy analysis

Numerous studies have shown that most GPP models can reproduce the spatial changes in GPP but failed to reproduce the temporal variations (Keenan et al., 2012; Yuan et al., 2014). Therefore, the capacity to reproduce realistic interannual variations for a GPP model is significantly important. In our study, the revised EC-LUE model performed a higher accuracy in reproducing the interannual variations in GPP than did the original EC-LUE model and other LUE models. Yuan et al. (2014) reported that the averaged slope of the regression relation between the mean annual GPP simulated by seven LUE models and the mean annual GPP estimated from EC tower data ranged from 0.19 to 0.56 (Fig. 4(c)). While the revised EC-LUE model showed a higher slope of regression relation (0.71), which is much closer to 1 than that obtained from other LUE models (Fig. 4(c)). The VPM GPP showed less interannual variation across most biomes ($R^2$ <0.5), probably because of the insensitivity of the environmental stress factors at the interannual scale (Zhang et al., 2017). In contrast, 74% of the sites showed higher $R^2$ values (>0.5) for the revised EC-LUE model. The improvements of the revised EC-LUE model in reproducing interannual variations are owing to the integration of several important environmental drivers for vegetation

https://doi.org/10.5194/essd-2019-126
Preprint. Discussion started: 7 August 2019


Open Access Earth System Science Data Discussions

production (i.e., atmospheric $CO_2$ concentration, radiation components, and VPD), which exhibited large variations and contributed significantly to vegetation production at interannual scale.

By integrating the atmospheric $CO_2$ concentration, the revised EC-LUE model suggested a $CO_2$ sensitivity ($\beta_{CO2}$) of 7.62 ± 0.04 Pg C per 100 ppm (Fig. 7(b)), which indicates an increase of 6.1% in GPP with a rise of 100 ppm in atmospheric [$CO_2$]. Our estimate is comparable to the observed response of NPP to the increased $CO_2$ in the FACE experiments (13% per 100 ppm) and estimates of other ecosystem models (5–20% per 100 ppm) (Piao et al., 2013). The elevated atmospheric $CO_2$ concentration substantially contributes to the vegetation productivity.

The evaporation fraction (EF), namely the ratio of evapotranspiration (ET) to net radiation (Rn), was used to indicate the water stress on vegetation growth in the original EC-LUE model (Yuan et al., 2007; 2010). While the atmospheric VPD was used to indicate water stress to avoid the aggregated errors from ET simulations in the revised EC-LUE model. Physiologically, vegetation production is sensitive to both atmospheric VPD and soil moisture availability to roots. Recent studies highlighted that the increase in VPD had a larger limitation to the surface conductance and evapotranspiration than soil moisture over short time scales in many biomes (Novick et al., 2016; Sulman et al., 2016). Other studies have also suggested substantial impacts of VPD on vegetation growth (de Cárcer et al., 2018; Ding et al., 2018), forest mortality (Williams et al., 2013), and crop yields (Lobell et al., 2014). It is increasingly important to integrate the atmospheric water constraint to the carbon and water flux modelling.

### 4.2 Comparison of global GPP product

Global GPP estimates remain highly uncertain despite the substantial advances in remote sensing technology, ground observations, and theory of carbon flux modeling (Zheng et al., 2018; Ryu et al., 2019). Our study showed large differences in the magnitude of global GPP estimated by various models varying from 92.7 to 168.7 Pg C $yr^{-1}$ (Figs. 8–9). The LUE models simulated the global GPP ranging from 92.7 to 133.7 Pg C $yr^{-1}$ (Fig. 9(a1)). Several machine learning approaches estimated the global GPP ranging from 108.9 to 144.2 Pg C $yr^{-1}$ (Fig. 9(a2)). A comparison of ten global terrestrial ecosystem models of TRENDY showed that the global GPP ranged from 118.6 to 168.7 Pg C $yr^{-1}$ (Fig. 9(a3)). The revised EC-LUE model quantified the mean global GPP from 1982 to 2017 as 125.3 ± 3.1 Pg C $yr^{-1}$. Other studies also support our conclusion that there are large uncertainties in the GPP estimates. By comparing diverse GPP models and products, Anav et al. (2015) reported that the global GPP ranged from 112 to 169 Pg C $yr^{-1}$. Seven satellite-based LUE models estimated the global GPP ranged from 95.1 to 139.7 Pg C $yr^{-1}$ over the period of 2000–2010 (Cai et al., 2014).

<<Figure 8>>

The interannual variability and trend in GPP also vary substantially with different models. This study showed that the interannual variability (standard deviation) ranged from 0.33 to 6.79 Pg C $yr^{-1}$, with the trends varying from −0.07 to 0.84 Pg C $yr^{-2}$ (Fig. 9). The biophysical models showed large interannual variability, with the standard deviation ranging from 1.38 to 6.79 Pg C $yr^{-1}$. The LUE models estimated the interannual variability varying from 1.30 to 3.13 Pg C $yr^{-1}$. In contrast, the machine learning models exhibited less interannual variability with standard deviation under 1.0 Pg C $yr^{-1}$. The interannual

https://doi.org/10.5194/essd-2019-126
Preprint. Discussion started: 7 August 2019




variability of the revised EC-LUE model was 3.1 Pg C $yr^{-1}$ (Figs. 9(b1)–(b3)). In general, the GPP interannual variability before year 2000 year was greater than that after year 2001 for most of the biophysical models and LUE models (Figs. 9(b1)–(b3)). Most GPP models showed increased trend or insignificant trend during all valid years and before 2000. Similar to the standard deviation, the trends of machine learning models were less than other models. Compared with the other models, CLASS and the revised EC-LUE model showed a significant decreasing trend after 2001 (Figs. 9(c1)–(c3)), probably because of the joint effect of increased VPD and decreased PAR (Fig. 7(c)).

<<Figure 9>>

### 4.3 Model uncertainty

The revised EC-LUE model showed the lowest accuracy for the evergreen broadleaf forests in the tropic areas (Figs. 2–3). Similarly, other satellite-based models exhibited a large uncertainty in the GPP simulations over tropical forest areas (Ryu et al., 2011; Yuan et al., 2014). MODIS GPP product (MOD17) underestimated the GPP at high productivity sites over the tropical evergreen forests (de Almeida et al., 2018). Regarding the quality of satellite data, a high cloud cover exists over tropical regions, introducing large uncertainties to FAPAR/LAI and other vegetation indices (e.g., NDVI and EVI). For example, less reliable MOD15 FAPAR data during January to April because of the cloudiness contamination, which could substantially affect the seasonality of GPP estimates (de Almeida et al., 2018). In addition, the quality of satellite data even affects the evaluation of the interannual variations. Saleska et al. (2007) reported that a large scale green-up in the Amazon evergreen forests during the drought in 2005 using MODIS EVI data. However, an opposite conclusion was arrived when cloud-contaminated data were excluded from the analysis, showing no obvious green-up in the Amazon evergreen forests during the drought in 2005 (Samanta et al., 2010). Additionally, several subsequent studies found increased LAI and EVI during the dry season in the Amazon evergreen forests; however, a recent study highlighted that the apparent seasonal changes in EVI result from the variations in the sun-sensor geometry rather than vegetation greenness (Morton et al., 2014). The latest study highlighted that the aggregate canopy phenology rather than the climate changes is the main causes of the seasonal changes in photosynthesis in evergreen broadleaf forests (Wu et al., 2016). In particularly, the new leaf growing synchronously with dry season litterfall may shift the old canopy to be younger, which can explain the significant seasonal increase (~27%) in the ecosystem photosynthesis. Therefore, the vertical changes in leaf age and photosynthesis ability with canopy depth are important to simulate the seasonal variations in carbon flux in tropical forests (Wu et al., 2017). These leaf trait related parameters can be simulated from narrow-band spectra of leaves (Serbin et al., 2012; Dechant et al., 2017). Nevertheless, because of the limitation in obtaining the large scale hyperspectral remote sensing data, regional or global estimation of these parameters are currently unavailable.

The revised EC-LUE model does not integrate the regulation of soil nitrogen content on vegetation production. Atmospheric nitrogen deposition has exhibited a large increasing trend in the past few decades because of the excessive fossil fuel combustion in the industrial and transportation sectors and the abuse of nitrogenous fertilizer in the agricultural practice (Galloway et al., 2004). And the global land atmospheric nitrogen deposition is expected to further increase dramatically

https://doi.org/10.5194/essd-2019-126
Preprint. Discussion started: 7 August 2019




from 25–40 Tg N $yr^{-1}$ in 2000s to 60–100 Tg N $yr^{-1}$ in 2100 (Lamarque et al., 2005). A meta-analysis of worldwide nitrogen addition experiments found that nitrogen addition could have a significantly positive effect on vegetation productivity (Liu and Greaver, 2009). As most terrestrial ecosystems are nitrogen limited, quantifying the spatio-temporal distributions of vegetation nitrogen content at large scales is essential to improve the accuracy of carbon flux estimation. Several studies quantified the leaf nitrogen content by detecting the nitrogen absorption spectra from the narrow-band of hyperspectral data (Cho, 2007). However, leaf water, starch, lignin, and cellulose overlap with the absorption characters of nitrogen in the shortwave infrared bands, making it difficult to retrieve the nitrogen content (Kokaly and Clark, 1999). Additionally, canopy structures, background, and the illumination/viewing geometry, can further decrease the capacity to detect leaf nitrogen (Yoder and Pettigrew-Crosby, 1995; Knyazikhin et al., 2013). Advances in inversion and statistical models of leaf or canopy nitrogen have emerged (Asner et al., 2011; Dechant et al., 2017; Wang et al., 2018), but these methods require further evaluation over large regions and the global map of leaf or canopy nitrogen is not available yet.

## 5 Data availability

The 0.05 ° × 0.05 ° global GPP dataset for 1982-2017 is available at https://doi.org/10.6084/m9.figshare.8942336 (Zheng et al., 2019). The dataset is provided in hdf format at 8-day interval. The valid value is ranged from 0 to 3000, and the background fill value is 65535. The scale factor of the data is 0.01. Each hdf file represents an 8-day GPP at daily value (unit: g C $m^{-2}$ $day^{-1}$). To obtain the summation of each 8-day (or 5-day or 6-day) period, please multiply the GPP value by corresponding days (8 for the first 45 values, and 5 or 6 for the last value in a year).

## 6 Conclusion

In this study, we produced a long-term global GPP dataset by integrating several major long-term environmental variables: atmospheric $CO_2$ concentration, radiation components, and atmospheric water vapor pressure. These environmental variables showed substantial long-term changes and contributed significantly to vegetation production at interannual scale. The revised EC-LUE performed well in simulating the spatial, seasonal, and interannual variations in global GPP. Particularly, it has a unique superiority in reproducing the interannual variations in GPP at both site level and global scales. Therefore, the GPP derived from the revised EC-LUE model provides an alternative and reliable estimates of global GPP at the long-term scale by integrating the important environmental variables.

https://doi.org/10.5194/essd-2019-126
Preprint. Discussion started: 7 August 2019




**Author contributions.** W. Yuan and Y. Zheng designed the research, performed the analysis, and wrote the paper; R. Shen, Y. Wang, and X. Li performed the analysis; S. Liu, S. Liang, J. Chen, W. Ju, and L. Zhang edited and revised the manuscript.

**Competing interests.** The authors declare that they have no conflict of interest.

## Acknowledgements

This study was supported by National Key Basic Research Program of China (2016YFA0602701), Changjiang Young Scholars Programme of China (Q2016161), Training Project of Sun Yat-sen University (16lgjc53), Fok Ying Tung Education Foundation (151015), and Beijing Normal University Project (2015KJJCA14). The covariance data used in the study was acquired and shared by the FLUXNET community.

## References

Ainsworth, E.A., Long, S.P.: What have we learned from 15 years of free-air $CO_2$ enrichment (FACE)? A meta-analytic review of the responses of photosynthesis, canopy, New Phytol., 165, 351-371, doi:10.1111/j.1469-8137.2004.01224.x, 2005.

Alton, P.B., North, P.R., Los, S.O.: The impact of diffuse sunlight on canopy light-use efficiency, gross photosynthetic product and net ecosystem exchange in three forest biomes, Global Change Biol., 13, 776-787, doi:10.1111/j.1365-2486.2007.01316.x, 2007.

Anav, A., Friedlingstein, P., Beer, C., Ciais, P., Harper, A., Jones, C., Murray-Tortarolo, G., Papale, D., Parazoo, N.C., Peylin, P., Piao, S., Sitch, S., Viovy, N., Wiltshire, A., Zhao, M.: Spatiotemporal patterns of terrestrial gross primary production: A review, Rev. Geophys., 53, 785-818, doi:10.1002/2015rg000483, 2015.

Asner, G.P., Martin, R.E., Knapp, D.E., Tupayachi, R., Anderson, C., Carranza, L., Martinez, P., Houcheime, M., Sinca, F., Weiss, P.: Spectroscopy of canopy chemicals in humid tropical forests, Remote Sens. Environ., 115, 3587-3598, doi:10.1016/j.rse.2011.08.020, 2011.

Cai, W., Yuan, W., Liang, S., Zhang, X., Dong, W., Xia, J., Fu, Y., Chen, Y., Liu, D., Zhang, Q.: Improved estimations of gross primary production using satellite-derived photosynthetically active radiation, J. Geophys. Res. G: Biogeosci., 119, 110-123, doi:10.1002/2013jg002456, 2014.

Cai, W., Yuan, W., Liang, S., Liu, S., Dong, W., Chen, Y., Liu, D., Zhang, H.: Large Differences in Terrestrial Vegetation Production Derived from Satellite-Based Light Use Efficiency Models, Remote Sens., 6, 8945-8965, doi:10.3390/rs6098945, 2014.

Canadell, J.G., Le Quere, C., Raupach, M.R., Field, C.B., Buitenhuis, E.T., Ciais, P., Conway, T.J., Gillett, N.P., Houghton, R.A., Marland, G.: Contributions to accelerating atmospheric $CO_2$ growth from economic activity, carbon intensity, and efficiency of natural sinks, Proc. Natl. Acad. Sci. U.S.A., 104, 18866-18870, doi:10.1073/pnas.0702737104, 2007.

https://doi.org/10.5194/essd-2019-126
Preprint. Discussion started: 7 August 2019


Chen, J.M., Liu, J., Cihlar, J., Goulden, M.L.: Daily canopy photosynthesis model through temporal and spatial scaling for remote sensing applications, Ecol. Modell., 124, 99-119, doi:10.1016/s0304-3800(99)00156-8, 1999.

Cho, M.A., Skidmore, A., Corsi, F., van Wieren, S.E., Sobhan, I.: Estimation of green grass/herb biomass from airborne hyperspectral imagery using spectral indices and partial least squares regression, International Journal of Applied Earth Observation and Geoinformation, 9, 414-424, doi:10.1016/j.jag.2007.02.001, 2007.

Collatz, G.J., Ball, J.T., Grivet, C., Berry, J.A.: Physiological and environmental regulation of stomatal conductance, photosynthesis and transpiration: a model that includes a laminar boundary layer, Agric. For. Meteorol., 54, 107-136, 1991.

de Almeida, C.T., Delgado, R.C., Galvao, L.S., de Oliveira Cruz e Aragao, L.E., Concepcion Ramos, M.: Improvements of the MODIS Gross Primary Productivity model based on a comprehensive uncertainty assessment over the Brazilian Amazonia, ISPRS J. Photogramm. Remote Sens., 145, 268-283, doi:10.1016/j.isprsjprs.2018.07.016, 2018.

de Cárcer, P.S., Vitasse, Y., Peñuelas, J., Jassey, V.E.J., Buttler, A., Signarbieux, C.: Vapor-pressure deficit and extreme climatic variables limit tree growth, Global Change Biol., 24, 1108-1122, doi:10.1111/gcb.13973, 2018.

Dechant, B., Cuntz, M., Vohland, M., Schulz, E., Doktor, D.: Estimation of photosynthesis traits from leaf reflectance spectra: Correlation to nitrogen content as the dominant mechanism, Remote Sens. Environ., 196, 279-292, doi:10.1016/j.rse.2017.05.019, 2017.

Ding, J., Yang, T., Zhao, Y., Liu, D., Wang, X., Yao, Y., Peng, S., Wang, T., Piao, S.: Increasingly Important Role of Atmospheric Aridity on Tibetan Alpine Grasslands, Geophys. Res. Lett., 45, 2852-2859, doi:10.1002/2017gl076803, 2018.

Farquhar, G.D., von Caemmerer, S., Berry, J.A.: A biochemical model of photosynthetic $CO_2$ assimilation in leaves of C 3 species, Planta, 149, 78-90, doi:10.1007/bf00386231, 1980.

Fletcher, A.L., Sinclair, T.R., Allen, L.H.: Transpiration responses to vapor pressure deficit in well watered 'slow-wilting' and commercial soybean, Environ. Exp. Bot., 61, 145-151, doi:10.1016/j.envexpbot.2007.05.004, 2007.

Galloway, J.N., Dentener, F.J., Capone, D.G., Boyer, E.W., Howarth, R.W., Seitzinger, S.P., Asner, G.P., Cleveland, C.C., Green, P.A., Holland, E.A., Karl, D.M., Michaels, A.F., Porter, J.H., Townsend, A.R., Vorosmarty, C.J.: Nitrogen cycles: past, present, and future, Biogeochemistry, 70, 153-226, doi:10.1007/s10533-004-0370-0, 2004.

Gilgen, H., Wild, M., Ohmura, A.: Means and trends of shortwave irradiance at the surface estimated from Global Energy Balance Archive data, J. Clim., 11, 2042-2061, doi:10.1175/1520-0442-11.8.2042, 1998.

Gu, L.H., Baldocchi, D., Verma, S.B., Black, T.A., Vesala, T., Falge, E.M., Dowty, P.R.: Advantages of diffuse radiation for terrestrial ecosystem productivity, J. Geophys. Res. D: Atmos., 10710.1029/2001jd001242, 2002.

Kanniah, K.D., Beringer, J., North, P., Hutley, L.: Control of atmospheric particles on diffuse radiation and terrestrial plant productivity: A review, Progress in Physical Geography-Earth and Environment, 36, 209-237, doi:10.1177/0309133311434244, 2012.

Ju, W., Chen, J.M., Black, T.A., Barr, A.G., Liu, J., Chen, B.: Modelling multi-year coupled carbon and water fluxes in a boreal aspen forest, Agric. For. Meteorol., 140, 136-151, doi:10.1016/j.agrformet.2006.08.008, 2006.

https://doi.org/10.5194/essd-2019-126
Preprint. Discussion started: 7 August 2019




Keenan, T.F., Baker, I., Barr, A., Ciais, P., Davis, K., Dietze, M., Dragon, D., Gough, C.M., Grant, R., Hollinger, D., Hufkens, K., Poulter, B., McCaughey, H., Raczka, B., Ryu, Y., Schaefer, K., Tian, H., Verbeeck, H., Zhao, M., Richardson, A.D.: Terrestrial biosphere model performance for inter-annual variability of land-atmosphere $CO_2$ exchange, Global Change Biol., 18, 1971-1987, doi:10.1111/j.1365-2486.2012.02678.x, 2012.

Keenan, T.F., Prentice, I.C., Canadell, J.G., Williams, C.A., Wang, H., Raupach, M., Collatz, G.J.: Recent pause in the growth rate of atmospheric $CO_2$ due to enhanced terrestrial carbon uptake, Nat. Commun., 710.1038/ncomms13428, 2016.

Knyazikhin, Y., Schull, M.A., Stenberg, P., Mottus, M., Rautiainen, M., Yang, Y., Marshak, A., Latorre Carmona, P., Kaufmann, R.K., Lewis, P., Disney, M.I., Vanderbilt, V., Davis, A.B., Baret, F., Jacquemoud, S., Lyapustin, A., Myneni, R.B.: Hyperspectral remote sensing of foliar nitrogen content, Proc. Natl. Acad. Sci. U.S.A., 110, E185-E192, doi:10.1073/pnas.1210196109, 2013.

Kokaly, R.F., Clark, R.N.: Spectroscopic determination of leaf biochemistry using band-depth analysis of absorption features and stepwise multiple linear regression, Remote Sens. Environ., 67, 267-287, doi:10.1016/s0034-4257(98)00084-4, 1999.

Konings, A.G., Williams, A.P., Gentine, P.: Sensitivity of grassland productivity to aridity controlled by stomatal and xylem regulation, Nat. Geosci., 10, 284-+, doi:10.1038/ngeo2903, 2017.

Korson, L., Drost-Hansen, W., Millero, F.J.: Viscosity of water at various temperatures, J. Phys. Chem., 73, 34-39, doi:10.1021/j100721a006, 1969.

Krupkova, L., Markova, I., Havrankova, K., Pokorny, R., Urban, O., Sigut, L., Pavelka, M., Cienciala, E., Marek, M.V.: Comparison of different approaches of radiation use efficiency of biomass formation estimation in Mountain Norway spruce, Trees-Structure and Function, 31, 325-337, doi:10.1007/s00468-016-1486-2, 2017.

Lamarque, J.F., Kiehl, J.T., Brasseur, G.P., Butler, T., Cameron-Smith, P., Collins, W.D., Collins, W.J., Granier, C., Hauglustaine, D., Hess, P.G., Holland, E.A., Horowitz, L., Lawrence, M.G., McKenna, D., Merilees, P., Prather, M.J., Rasch, P.J., Rotman, D., Shindell, D., Thornton, P.: Assessing future nitrogen deposition and carbon cycle feedback using a multimodel approach: Analysis of nitrogen deposition, J. Geophys. Res. D: Atmos., 11010.1029/2005jd005825, 2005.

Li, X.L., Liang, S.L., Yu, G.R., Yuan, W.P., Cheng, X., Xia, J.Z., Zhao, T.B., Feng, J.M., Ma, Z.G., Ma, M.G., Liu, S.M., Chen, J.Q., Shao, C.L., Li, S.G., Zhang, X.D., Zhang, Z.Q., Chen, S.P., Ohta, T., Varlagin, A., Miyata, A., Takagi, K., Saiqusa, N., Kato, T.: Estimation of gross primary production over the terrestrial ecosystems in China, Ecol. Modell., 261, 80-92, doi:10.1016/j.ecolmodel.2013.03.024, 2013.

Liu, L., Greaver, T.L.: A review of nitrogen enrichment effects on three biogenic GHGs: the $CO_2$ sink may be largely offset by stimulated N2O and CH4 emission, Ecol. Lett., 12, 1103-1117, doi:10.1111/j.1461-0248.2009.01351.x, 2009.

Liu, S., Bond-Lamberty, B., Boysen, L.R., Ford, J.D., Fox, A., Gallo, K., Hatfield, J., Henebry, G.M., Huntington, T.G., Liu, Z., Loveland, T.R., Norby, R.J., Sohl, T., Steiner, A.L., Yuan, W., Zhang, Z., Zhao, S.: Grand Challenges in Understanding the Interplay of Climate and Land Changes, Earth Interactions, 21, 1-43, doi:10.1175/ei-d-16-0012.1, 2017.

https://doi.org/10.5194/essd-2019-126
Preprint. Discussion started: 7 August 2019


Liu, Y., Xiao, J., Ju, W., Zhu, G., Wu, X., Fan, W., Li, D., Zhou, Y.: Satellite-derived LAI products exhibit large discrepancies and can lead to substantial uncertainty in simulated carbon and water fluxes, Remote Sens. Environ., 206, 174-188, doi:10.1016/j.rse.2017.12.024, 2018.

Lobell, D.B., Roberts, M.J., Schlenker, W., Braun, N., Little, B.B., Rejesus, R.M., Hammer, G.L.: Greater Sensitivity to Drought Accompanies Maize Yield Increase in the US Midwest, Science, 344, 516-519, doi:10.1126/science.1251423, 2014.

Monteith, J.: Solar radiation and productivity in tropical ecosystems, J. Appl. Ecol., 9, 747-766, 1972.

Morton, D.C., Nagol, J., Carabajal, C.C., Rosette, J., Palace, M., Cook, B.D., Vermote, E.F., Harding, D.J., North, P.R.J.: Amazon forests maintain consistent canopy structure and greenness during the dry season, Nature, 506, 221-+, doi:10.1038/nature13006, 2014.

Norby, R.J., DeLucia, E.H., Gielen, B., Calfapietra, C., Giardina, C.P., King, J.S., Ledford, J., McCarthy, H.R., Moore, D.J.P., Ceulemans, R., De Angelis, P., Finzi, A.C., Karnosky, D.F., Kubiske, M.E., Lukac, M., Pregitzer, K.S., Scarascia-Mugnozza, G.E., Schlesinger, W.H., Oren, R.: Forest response to elevated $CO_2$ is conserved across a broad range of productivity, Proc. Natl. Acad. Sci. U.S.A., 102, 18052-18056, doi:10.1073/pnas.0509478102, 2005.

Norby, R.J., Wullschleger, S.D., Gunderson, C.A., Johnson, D.W., Ceulemans, R.: Tree responses to rising $CO_2$ in field experiments: implications for the future forest, Plant Cell Environ., 22, 683-714, doi:10.1046/j.1365-3040.1999.00391.x, 1999.

Piao, S., Sitch, S., Ciais, P., Friedlingstein, P., Peylin, P., Wang, X., Ahlstrom, A., Anav, A., Canadell, J.G., Cong, N., Huntingford, C., Jung, M., Levis, S., Levy, P.E., Li, J., Lin, X., Lomas, M.R., Lu, M., Luo, Y., Ma, Y., Myneni, R.B., Poulter, B., Sun, Z., Wang, T., Viovy, N., Zaehle, S., Zeng, N.: Evaluation of terrestrial carbon cycle models for their response to climate variability and to $CO_2$ trends, Global Change Biol., 19, 2117-2132, doi:10.1111/gcb.12187, 2013.

Pierce, D.W., Westerling, A.L., Oyler, J.: Future humidity trends over the western United States in the CMIP5 global climate models and variable infiltration capacity hydrological modeling system, Hydrol. Earth Syst. Sci., 17, 1833-1850, doi:10.5194/hess-17-1833-2013, 2013.

Potter, C.S., Randerson, J.T., Field, C.B., Matson, P.A., Vitousek, P.M., Mooney, H.A., Klooster, S.A.: Terrestrial ecosystem production: A process model-based on global satellite and surface data, Global Biogeochem. Cycles, 7, 811-841, doi:10.1029/93gb02725, 1993.

Prentice, I.C., Dong, N., Gleason, S.M., Maire, V., Wright, I.J.: Balancing the costs of carbon gain and water transport: testing a new theoretical framework for plant functional ecology, Ecol. Lett., 17, 82-91, doi:10.1111/ele.12211, 2014.

Rawson, H.M., Begg, J.E., Woodward, R.G.: The effect of atmospheric humidity on photosynthesis, transpiration and water use efficiency of leaves of several plant species, Planta, 134, 5-10, doi:10.1007/bf00390086, 1977.

Reichstein, M., Falge, E., Baldocchi, D., Papale, D., Aubinet, M., Berbigier, P., Bernhofer, C., Buchmann, N., Gilmanov, T., Granier, A., Grunwald, T., Havrankova, K., Ilvesniemi, H., Janous, D., Knohl, A., Laurila, T., Lohila, A., Loustau, D., Matteucci, G., Meyers, T., Miglietta, F., Ourcival, J.-M., Pumpanen, J., Rambal, S., Rotenberg, E., Sanz, M., Tenhunen, J., Seufert, G., Vaccari, F., Vesala, T., Yakir, D., Valentini, R.: On the separation of net ecosystem exchange into assimilation

https://doi.org/10.5194/essd-2019-126
Preprint. Discussion started: 7 August 2019




and ecosystem respiration: review and improved algorithm, Global Change Biol., 11, 1424-1439, doi:10.1111/j.1365-2486.2005.001002.x, 2005.

Rienecker, M.M., Suarez, M.J., Gelaro, R., Todling, R., Bacmeister, J., Liu, E., Bosilovich, M.G., Schubert, S.D., Takacs, L., Kim, G.-K., Bloom, S., Chen, J., Collins, D., Conaty, A., Da Silva, A., Gu, W., Joiner, J., Koster, R.D., Lucchesi, R., Molod, A., Owens, T., Pawson, S., Pegion, P., Redder, C.R., Reichle, R., Robertson, F.R., Ruddick, A.G., Sienkiewicz, M., Woollen, J.: MERRA: NASA's modern-era retrospective analysis for research and applications, J. Clim., 24, 3624-3648, doi:10.1175/jcli-d-11-00015.1, 2011.

Running, S.W., Nemani, R.R., Heinsch, F.A., Zhao, M.S., Reeves, M., Hashimoto, H.: A continuous satellite-derived measure of global terrestrial primary production, Bioscience, 54, 547-560, doi:10.1641/0006-3568(2004)054[0547:acsmog]2.0.co;2, 2004.

Ryu, Y., Baldocchi, D.D., Kobayashi, H., van Ingen, C., Li, J., Black, T.A., Beringer, J., van Gorsel, E., Knohl, A., Law, B.E., Roupsard, O.: Integration of MODIS land and atmosphere products with a coupled-process model to estimate gross primary productivity and evapotranspiration from 1 km to global scales, Global Biogeochem. Cycles, 2510.1029/2011gb004053, 2011.

Ryu, Y., Berry, J.A., Baldocchi, D.D.: What is global photosynthesis? History, uncertainties and opportunities, Remote Sens. Environ., 223, 95-114, doi:10.1016/j.rse.2019.01.016, 2019.

Saleska, S.R., Didan, K., Huete, A.R., da Rocha, H.R.: Amazon forests green-up during 2005 drought, Science, 318, 612-612, doi:10.1126/science.1146663, 2007.

Samanta, A., Ganguly, S., Hashimoto, H., Devadiga, S., Vermote, E., Knyazikhin, Y., Nemani, R.R., Myneni, R.B.: Amazon forests did not green-up during the 2005 drought, Geophys. Res. Lett., 3710.1029/2009gl042154, 2010.

Serbin, S.P., Dillaway, D.N., Kruger, E.L., Townsend, P.A.: Leaf optical properties reflect variation in photosynthetic metabolism and its sensitivity to temperature, J. Exp. Bot., 63, 489-502, doi:10.1093/jxb/err294, 2012.

Simmons, A.J., Willett, K.M., Jones, P.D., Thorne, P.W., Dee, D.P.: Low-frequency variations in surface atmospheric humidity, temperature, and precipitation: Inferences from reanalyses and monthly gridded observational data sets, J. Geophys. Res. D: Atmos., 11510.1029/2009jd012442, 2010.

Smith, W.K., Reed, S.C., Cleveland, C.C., Ballantyne, A.P., Anderegg, W.R.L., Wieder, W.R., Liu, Y.Y., Running, S.W.: Large divergence of satellite and Earth system model estimates of global terrestrial $CO_2$ fertilization, Nat. Clim. Change, 6, 306-310, doi:10.1038/nclimate2879, 2016.

Stocker, B.D., Zscheischler, J., Keenan, T.F., Prentice, I.C., Seneviratne, S.I., Peñuelas, J.: Drought impacts on terrestrial primary production underestimated by satellite monitoring, Nat. Geosci., 12, 264-270, doi:10.1038/s41561-019-0318-6, 2019.

Sulman, B.N., Roman, D.T., Yi, K., Wang, L., Phillips, R.P., Novick, K.A.: High atmospheric demand for water can limit forest carbon uptake and transpiration as severely as dry soil, Geophys. Res. Lett., 43, 9686-9695, doi:10.1002/2016gl069416, 2016.

https://doi.org/10.5194/essd-2019-126
Preprint. Discussion started: 7 August 2019


Tang, S., Chen, J.M., Zhu, Q., Li, X., Chen, M., Sun, R., Zhou, Y., Deng, F., Xie, D.: LAI inversion algorithm based on directional reflectance kernels, J. Environ. Manage., 85, 638-648, doi:10.1016/j.jenvman.2006.08.018, 2007.

Urban, O., Janous, D., Acosta, M., Czerny, R., Markova, I., Navratil, M., Pavelka, M., Pokorny, R., Sprtova, M., Zhang, R., Spunda, V., Grace, J., Marek, M.V.: Ecophysiological controls over the net ecosystem exchange of mountain spruce stand. Comparison of the response in direct vs. diffuse solar radiation, Global Change Biol., 13, 157-168, doi:10.1111/j.1365-2486.2006.01265.x, 2007.

Van Wijngaarden, W.A., Vincent, L.A.: Trends in relative humidity in Canada from 1953–2003. In 15th Symp. on Global Change and Climate Variations, 2004.

Vuichard, N., Papale, D.: Filling the gaps in meteorological continuous data measured at FLUXNET sites with ERA-Interim reanalysis, Earth Syst. Sci. Data, 7, 157-171, doi:10.5194/essd-7-157-2015, 2015.

Wang, Z., Skidmore, A.K., Darvishzadeh, R., Wang, T.: Mapping forest canopy nitrogen content by inversion of coupled leaf-canopy radiative transfer models from airborne hyperspectral imagery, Agric. For. Meteorol., 253, 247-260, doi:10.1016/j.agrformet.2018.02.010, 2018.

Wild, M., Gilgen, H., Roesch, A., Ohmura, A., Long, C.N., Dutton, E.G., Forgan, B., Kallis, A., Russak, V., Tsvetkov, A.: From dimming to brightening: Decadal changes in solar radiation at Earth's surface, Science, 308, 847-850, doi:10.1126/science.1103215, 2005.

Willett, K.M., Dunn, R.J.H., Thorne, P.W., Bell, S., de Podesta, M., Parker, D.E., Jones, P.D., Williams, C.N., Jr.: HadISDH land surface multi-variable humidity and temperature record for climate monitoring, Climate of the Past, 10, 1983-2006, doi:10.5194/cp-10-1983-2014, 2014.

Williams, A.P., Allen, C.D., Macalady, A.K., Griffin, D., Woodhouse, C.A., Meko, D.M., Swetnam, T.W., Rauscher, S.A., Seager, R., Grissino-Mayer, H.D., Dean, J.S., Cook, E.R., Gangodagamage, C., Cai, M., McDowell, N.G.: Temperature as a potent driver of regional forest drought stress and tree mortality, Nat. Clim. Change, 3, 292-297, doi:10.1038/nclimate1693, 2013.

Wu, J., Albert, L.P., Lopes, A.P., Restrepo-Coupe, N., Hayek, M., Wiedemann, K.T., Guan, K., Stark, S.C., Christoffersen, B., Prohaska, N., Tavares, J.V., Marostica, S., Kobayashi, H., Ferreira, M.L., Campos, K.S., da Silva, R., Brando, P.M., Dye, D.G., Huxman, T.E., Huete, A.R., Nelson, B.W., Saleska, S.R.: Leaf development and demography explain photosynthetic seasonality in Amazon evergreen forests, Science, 351, 972-976, doi:10.1126/science.aad5068, 2016.

Wu, J., Guan, K., Hayek, M., Restrepo-Coupe, N., Wiedemann, K.T., Xu, X., Wehr, R., Christoffersen, B.O., Miao, G., da Silva, R., de Araujo, A.C., Oliviera, R.C., Camargo, P.B., Monson, R.K., Huete, A.R., Saleska, S.R.: Partitioning controls on Amazon forest photosynthesis between environmental and biotic factors at hourly to interannual timescales, Global Change Biol., 23, 1240-1257, doi:10.1111/gcb.13509, 2017.

Xiao, X.M., Zhang, Q.Y., Hollinger, D., Aber, J., Moore, B.: Modeling gross primary production of an evergreen needleleaf forest using modis and climate data, Ecol. Appl., 15, 954-969, doi:10.1890/04-0470, 2005.

https://doi.org/10.5194/essd-2019-126
Preprint. Discussion started: 7 August 2019




570 Xiao, Z., Liang, S., Wang, J., Xiang, Y., Zhao, X., Song, J.: Long-Time-Series Global Land Surface Satellite Leaf Area Index Product Derived From MODIS and AVHRR Surface Reflectance, IEEE Trans. Geosci. Remote Sens., 54, 5301-5318, doi:10.1109/tgrs.2016.2560522, 2016.

Xu, B., Li, J., Park, T., Liu, Q., Zeng, Y., Yin, G., Zhao, J., Fan, W., Yang, L., Knyazikhin, Y., Myneni, R.B.: An integrated method for validating long-term leaf area index products using global networks of site-based measurements, Remote Sens. 575 Environ., 209, 134-151, doi:10.1016/j.rse.2018.02.049, 2018.

Yoder, B.J., Pettigrew-Crosby, R.E.: Predicting nitrogen and chlorophyll content and concentrations from reflectance spectra (400-2500 nm) at leaf and canopy scales, Remote Sens. Environ., 53, 199-211, doi:10.1016/0034-4257(95)00135-n, 1995.

Yuan, W., Cai, W., Xia, J., Chen, J., Liu, S., Dong, W., Merbold, L., Law, B., Arain, A., Beringer, J., Bernhofer, C., Black, A., Blanken, P.D., Cescatti, A., Chen, Y., Francois, L., Gianelle, D., Janssens, I.A., Jung, M., Kato, T., Kiely, G., Liu, D., 580 Marcolla, B., Montagnani, L., Raschi, A., Roupsard, O., Varlagin, A., Wohlfahrt, G.: Global comparison of light use efficiency models for simulating terrestrial vegetation gross primary production based on the La Thuile database, Agric. For. Meteorol., 192, 108-120, doi:10.1016/j.agrformet.2014.03.007, 2014.

Yuan, W., Liu, S., Zhou, G., Zhou, G., Tieszen, L.L., Baldocchi, D., Bernhofer, C., Gholz, H., Goldstein, A.H., Goulden, M.L., Hollinger, D.Y., Hu, Y., Law, B.E., Stoy, P.C., Vesala, T., Wofsy, S.C., AmeriFlux, C.: Deriving a light use efficiency 585 model from eddy covariance flux data for predicting daily gross primary production across biomes, Agric. For. Meteorol., 143, 189-207, doi:10.1016/j.agrformet.2006.12.001, 2007.

Yuan, W., Luo, Y., Li, X., Liu, S., Yu, G., Zhou, T., Bahn, M., Black, A., Desai, A.R., Cescatti, A., Marcolla, B., Jacobs, C., Chen, J., Aurela, M., Bernhofer, C., Gielen, B., Bohrer, G., Cook, D.R., Dragoni, D., Dunn, A.L., Gianelle, D., Gruenwald, T., Ibrom, A., Leclerc, M.Y., Lindroth, A., Liu, H., Marchesini, L.B., Montagnani, L., Pita, G., Rodeghiero, M., Rodrigues, 590 A., Starr, G., Stoy, P.C.: Redefinition and global estimation of basal ecosystem respiration rate, Global Biogeochem. Cycles, 2510.1029/2011gb004150, 2011.

Yuan, W., Liu, S., Yu, G., Bonnefond, J.-M., Chen, J., Davis, K., Desai, A.R., Goldstein, A.H., Gianelle, D., Rossi, F., Suyker, A.E., Verma, S.B.: Global estimates of evapotranspiration and gross primary production based on MODIS and global meteorology data, Remote Sens. Environ., 114, 1416-1431, doi:10.1016/j.rse.2010.01.022, 2010.

595 Zhang, Y., Xiao, X., Wu, X., Zhou, S., Zhang, G., Qin, Y., Dong, J.: Data Descriptor: A global moderate resolution dataset of gross primary production of vegetation for 2000-2016, Scientific Data, 410.1038/sdata.2017.165, 2017.

Zhao, M., Running, S.W.: Drought-Induced Reduction in Global Terrestrial Net Primary Production from 2000 Through 2009, Science, 329, 940-943, doi:10.1126/science.1192666, 2010.

Zheng, Y., Shen, R.; Wang, Y., Li, X., Liu, S., Liang, S., Chen, Jing M., Ju, W., Zhang, L., Yuan, W.: Improved estimate of 600 global gross primary production for reproducing its long-term variation, 1982-2017. figshare. Dataset. doi:10.6084/m9.figshare.8942336, 2019.

https://doi.org/10.5194/essd-2019-126
Preprint. Discussion started: 7 August 2019




Zheng, Y., Zhang, L., Xiao, J., Yuan, W., Yan, M., Li, T., Zhang, Z.: Sources of uncertainty in gross primary productivity simulated by light use efficiency models: Model structure, parameters, input data, and spatial resolution, Agric. For. Meteorol., 263, 242-257, doi:10.1016/j.agrformet.2018.08.003, 2018.

Zhu, Z., Piao, S., Myneni, R.B., Huang, M., Zeng, Z., Canadell, J.G., Ciais, P., Sitch, S., Friedlingstein, P., Arneth, A., Cao, C., Cheng, L., Kato, E., Koven, C., Li, Y., Lian, X., Liu, Y., Liu, R., Mao, J., Pan, Y., Peng, S., Penuelas, J., Poulter, B., Pugh, T.A.M., Stocker, B.D., Viovy, N., Wang, X., Wang, Y., Xiao, Z., Yang, H., Zaehle, S., Zeng, N.: Greening of the Earth and its drivers, Nat. Clim. Change, 6, 791-796, doi:10.1038/nclimate3004, 2016.

https://doi.org/10.5194/essd-2019-126
Preprint. Discussion started: 7 August 2019


Open Access Earth System Science Data Discussions

610 **Tables**

**Table 1: Information on the eddy covariance (EC) sites used in this study for model calibration and validation.**

| Site Name | Latitude | Longitude | Vegetation Type | Study Period |
|---|---|---|---|---|
| | | *Model calibration* | | |
| FI-Jok | 60.90ºN | 23.51ºE | CRO-C3 | 2000-2003 |
| US-Ne3 | 41.17ºN | 96.43ºW | CRO-C3/C4 | 2001-2011 |
| *US-ARM | 36.61ºN | 97.49ºW | CRO-C3/C4 | 2003-2012 |
| *FR-Gri | 48.84ºN | 1.95ºE | CRO-C4 | 2004-2011 |
| DE-Kli | 50.89ºN | 13.52ºE | CRO-C4 | 2004-2011 |
| US-KS2 | 28.61ºN | 80.67ºW | SHR | 2003-2006 |
| *DK-Sor | 55.49ºN | 11.64ºE | DBF | 1996-2014 |
| *US-UMB | 45.56ºN | 84.71ºW | DBF | 2000-2011 |
| CA-TPD | 42.64ºN | 80.56ºW | DBF | 2012-2014 |
| *DE-Hai | 51.08ºN | 10.45ºE | DBF | 2000-2011 |
| *US-Ha1 | 42.54ºN | 72.17ºW | DBF | 1991-2011 |
| *US-MMS | 39.32ºN | 86.41ºW | DBF | 1999-2011 |
| *US-Oho | 41.55ºN | 83.84ºW | DBF | 2004-2011 |
| CN-Din | 23.17ºN | 112.54ºE | EBF | 2003-2005 |
| *GF-Guy | 5.28ºN | 52.92ºW | EBF | 2004-2014 |
| *BR-Sa1 | 2.86ºS | 54.96ºW | EBF | 2008-2011 |
| IT-La2 | 45.95ºN | 11.29ºE | ENF | 2001 |
| *CA-Qfo | 49.69ºN | 74.34ºW | ENF | 2003-2010 |
| *US-NR1 | 40.03ºN | 105.55ºW | ENF | 1999-2011 |
| *RU-Fyo | 56.46ºN | 32.92ºE | ENF | 1998-2011 |
| *CA-NS2 | 55.91ºN | 98.52ºW | ENF | 2001-2005 |
| *NL-Loo | 52.17ºN | 5.74ºE | ENF | 1996-2011 |
| *DE-Obe | 50.78ºN | 13.72ºE | ENF | 2008-2011 |
| *FI-Hyy | 61.85ºN | 24.30ºE | ENF | 1996-2011 |
| US-Me6 | 44.32ºN | 121.61ºW | ENF | 2010-2011 |
| CA-SF1 | 54.49ºN | 105.82ºW | ENF | 2003-2006 |
| *CZ-BK1 | 49.50ºN | 18.54ºE | ENF | 2004-2011 |
| *CA-SF2 | 54.25ºN | 105.88ºW | ENF | 2001-2005 |

https://doi.org/10.5194/essd-2019-126
Preprint. Discussion started: 7 August 2019




| | | | | |
|---|---|---|---|---|
| CA-NS4 | 55.91°N | 98.38°W | ENF | 2003-2005 |
| CN-HaM | 37.37°N | 101.18°E | GRA | 2002-2004 |
| US-IB2 | 41.84°N | 88.24°W | GRA | 2004-2011 |
| CN-Du2 | 42.05°N | 116.28°E | GRA | 2007-2008 |
| CN-Cng | 44.59°N | 123.51°E | GRA | 2007-2010 |
| *CH-Cha | 47.21°N | 8.41°E | GRA | 2006-2008; 2010-2011 |
| *CH-Oe1 | 47.29°N | 7.73°E | GRA | 2002-2008 |
| CN-Cha | 42.40°N | 128.10°E | MF | 2003-2005 |
| *CA-Gro | 48.22°N | 82.16°W | MF | 2003-2011 |
| *US-PFa | 45.95°N | 90.27°W | MF | 1996-2011 |
| CN-Ha2 | 37.61°N | 101.33°E | WET | 2003-2005 |
| RU-Che | 68.61°N | 161.34°E | WET | 2002-2005 |
| US-WPT | 41.46°N | 83.00°W | WET | 2011-2013 |
| *US-Ton | 38.43°N | 120.97°W | SAV | 2001-2011 |
| | | *Model validation* | | |
| *US-Ne2 | 41.16°N | 96.47°W | CRO-C3/C4 | 2001-2011 |
| *DE-Kli | 50.89°N | 13.52°E | CRO-C3 | 2004-2014 |
| *US-Ne1 | 41.16°N | 96.47°W | CRO-C4 | 2001-2011 |
| DE-RuS | 50.87°N | 6.45°E | CRO-C4 | 2011-2014 |
| *US-UMd | 45.56°N | 84.70°W | DBF | 2007-2014 |
| *US-WCr | 45.81°N | 90.08°W | DBF | 1999-2006 |
| *FR-Fon | 48.48°N | 2.78°E | DBF | 2005-2011 |
| JP-MBF | 44.39°N | 142.32°E | DBF | 2004-2005 |
| IT-PT1 | 45.20°N | 9.06°E | DBF | 2002-2004 |
| *IT-Ro2 | 42.39°N | 11.92°E | DBF | 2002-2011 |
| *FR-Pue | 43.74°N | 3.60°E | EBF | 2000-2011 |
| MY-PSO | 2.97°N | 102.31°E | EBF | 2003-2009 |
| BR-Sa3 | 3.02°S | 54.97°W | EBF | 2000-2003 |
| *IT-Lav | 45.96°N | 11.28°E | ENF | 2003-2011 |
| *IT-Ren | 46.59°N | 11.43°E | ENF | 1999-2004; 2009-2011 |
| *CA-NS5 | 55.86°N | 98.49°W | ENF | 2001-2005 |
| *DE-Tha | 50.96°N | 13.57°E | ENF | 1997-2011 |
| *CA-TP3 | 42.71°N | 80.35°W | ENF | 2003-2011 |

https://doi.org/10.5194/essd-2019-126
Preprint. Discussion started: 7 August 2019




| | | | | |
|---|---|---|---|---|
| *CA-TP1 | 42.66°N | 80.56°W | ENF | 2003-2011 |
| CA-NS3 | 55.91°N | 98.38°W | ENF | 2001-2005 |
| CA-NS1 | 55.88°N | 98.48°W | ENF | 2002-2005 |
| DE-Lkb | 49.10°N | 13.30°E | ENF | 2009-2011 |
| *US-Me2 | 44.45°N | 121.56°W | ENF | 2002-2011 |
| *IT-SRo | 43.73°N | 10.28°E | ENF | 1999-2012 |
| CN-Qia | 26.74°N | 115.06°E | ENF | 2003-2005 |
| *CA-TP2 | 42.77°N | 80.46°W | ENF | 2003-2007 |
| *US-Blo | 38.90°N | 120.63°W | ENF | 1997-2007 |
| RU-Ha1 | 54.73°N | 90.00°E | GRA | 2002-2004 |
| *CH-Fru | 47.12°N | 8.54°E | GRA | 2006-2008; 2010-2011 |
| *CZ-BK2 | 49.49°N | 18.54°E | GRA | 2006-2011 |
| *NL-Hor | 52.24°N | 5.07°E | GRA | 2004-2011 |
| *US-Goo | 34.25°N | 89.87°W | GRA | 2002-2006 |
| US-AR2 | 36.64°N | 99.60°W | GRA | 2009-2011 |
| US-AR1 | 36.43°N | 99.42°W | GRA | 2009-2011 |
| *BE-Vie | 50.31°N | 6.00°E | MF | 1999-2011 |
| US-Syv | 46.24°N | 89.35°W | MF | 2001-2006 |
| *BE-Bra | 51.31°N | 4.52°E | MF | 1999-2011 |
| JP-SMF | 35.26°N | 137.08°E | MF | 2002-2006 |
| US-Ivo | 68.49°N | 155.75°W | WET | 2004-2007 |
| DE-Akm | 53.87°N | 13.68°E | WET | 2009-2014 |
| DE-Spw | 51.89°N | 14.03°E | WET | 2010-2011 |
| *US-Los | 46.08°N | 89.98°W | WET | 2000-2010 |
| DE-SfN | 47.81°N | 11.33°E | WET | 2012-2014 |

* indicates the site was used to investigate the interannual variations in GPP with observations greater than 5-years.

https://doi.org/10.5194/essd-2019-126
Preprint. Discussion started: 7 August 2019


Open Access Earth System Science Data Discussions

615 **Table 2: Input data used to drive the revised EC-LUE model.**

| Variable | Dataset/provider | Source |
|---|---|---|
| Air temperature | MERRA2 | https://gmao.gsfc.nasa.gov/reanalysis/MERRA-2/ |
| Dew point temperature | MERRA2 | https://gmao.gsfc.nasa.gov/reanalysis/MERRA-2/ |
| Direct PAR | MERRA2 | https://gmao.gsfc.nasa.gov/reanalysis/MERRA-2/ |
| Diffuse PAR | MERRA2 | https://gmao.gsfc.nasa.gov/reanalysis/MERRA-2/ |
| LAI | GLASS | http://www.glass.umd.edu/Download.html |
| Landcover map | MCD12Q1 | https://lpdaac.usgs.gov/products/mcd12q1v006/ |
| $CO_2$ concentration | NOAA's Earth System Research Laboratory | www.esrl.noaa.gov/gmd/ccgg/trends/ |

**Table 3: Optimized parameters ($\varepsilon_{msu}$, $\varepsilon_{msh}$, $\varphi$, and $VPD_0$) of the revised EC-LUE model for different vegetation types.**

| Vegetation Types | DBF | ENF | EBF | MF | GRA | CRO-C3 | CRO-C4 | SAV | SHR | WET |
|---|---|---|---|---|---|---|---|---|---|---|
| $\varepsilon_{msu}$ (g C $MJ^{-1}$) | 1.16 | 1.80 | 1.71 | 1.16 | 0.83 | 1.17 | 2.35 | 2.05 | 0.86 | 1.23 |
| $\varepsilon_{msh}$ (g C $MJ^{-1}$) | 3.33 | 3.95 | 3.97 | 3.16 | 1.75 | 2.38 | 5.54 | 3.95 | 2.42 | 2.45 |
| $\varphi$ (ppm) | 32 | 25 | 20 | 49 | 57 | 43 | 54 | 54 | 34 | 36 |
| $VPD_0$ (kPa) | 0.93 | 0.72 | 0.44 | 0.58 | 1.31 | 0.82 | 0.94 | 1.24 | 1.23 | 0.42 |

620

https://doi.org/10.5194/essd-2019-126
Preprint. Discussion started: 7 August 2019


Open Access Earth System Science Data Discussions

**Figures**

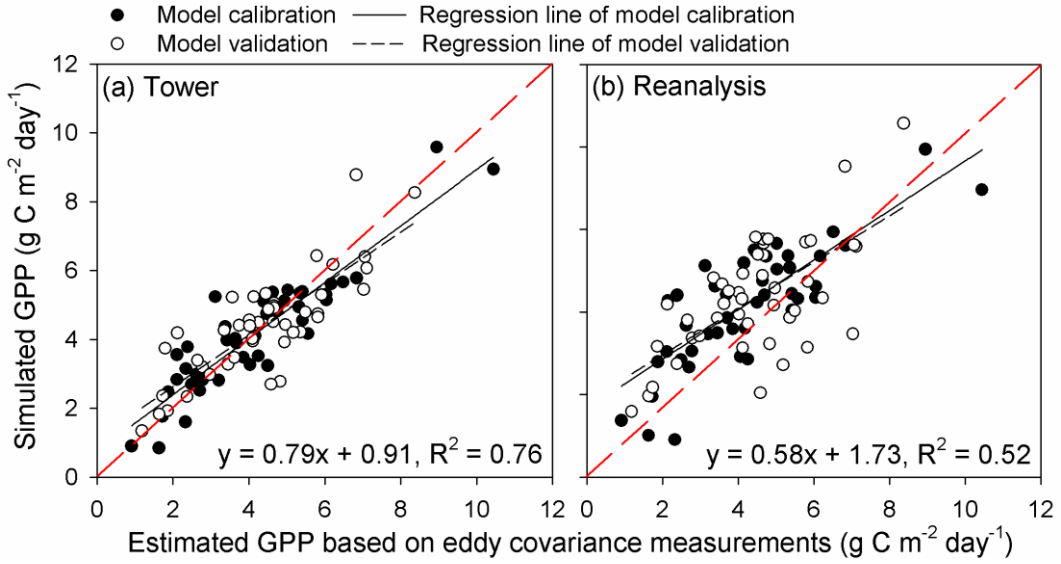


**Figure 1: Comparisons between annual mean GPP estimated from EC towers and annual mean GPP simulated by the revised EC-LUE model. The modeled GPP were simulated using (a) tower-derived meteorology (calibration: y = 0.82x + 0.75, $R^2$ = 0.83; validation: y = 0.75x + 1.13, $R^2$ = 0.68) and (b) global reanalysis meteorology (calibration: y = 0.60x + 1.66, $R^2$ = 0.62; validation: y = 0.56x + 1.84, $R^2$ = 0.40). The black lines are the regression lines, and the red dash lines are the 1:1 lines. The insert equations are the regression equations derived from all the sites.**

https://doi.org/10.5194/essd-2019-126
Preprint. Discussion started: 7 August 2019


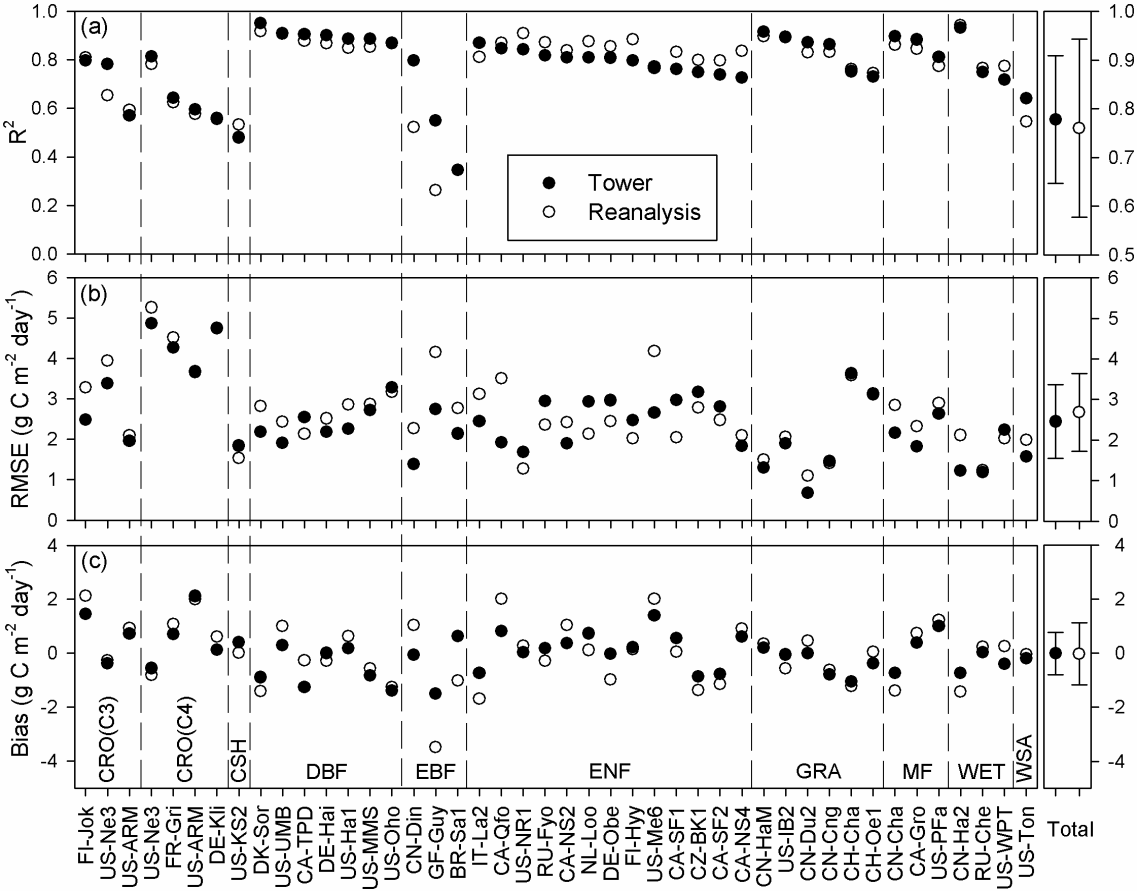


630 **Figure 2: Comparisons of 8-day mean GPP between the observations at 42 calibration sites and the model simulations. Solid and open dots indicate the GPP simulations derived from tower-derived meteorology data and meteorological reanalysis dataset, respectively.**

https://doi.org/10.5194/essd-2019-126
Preprint. Discussion started: 7 August 2019


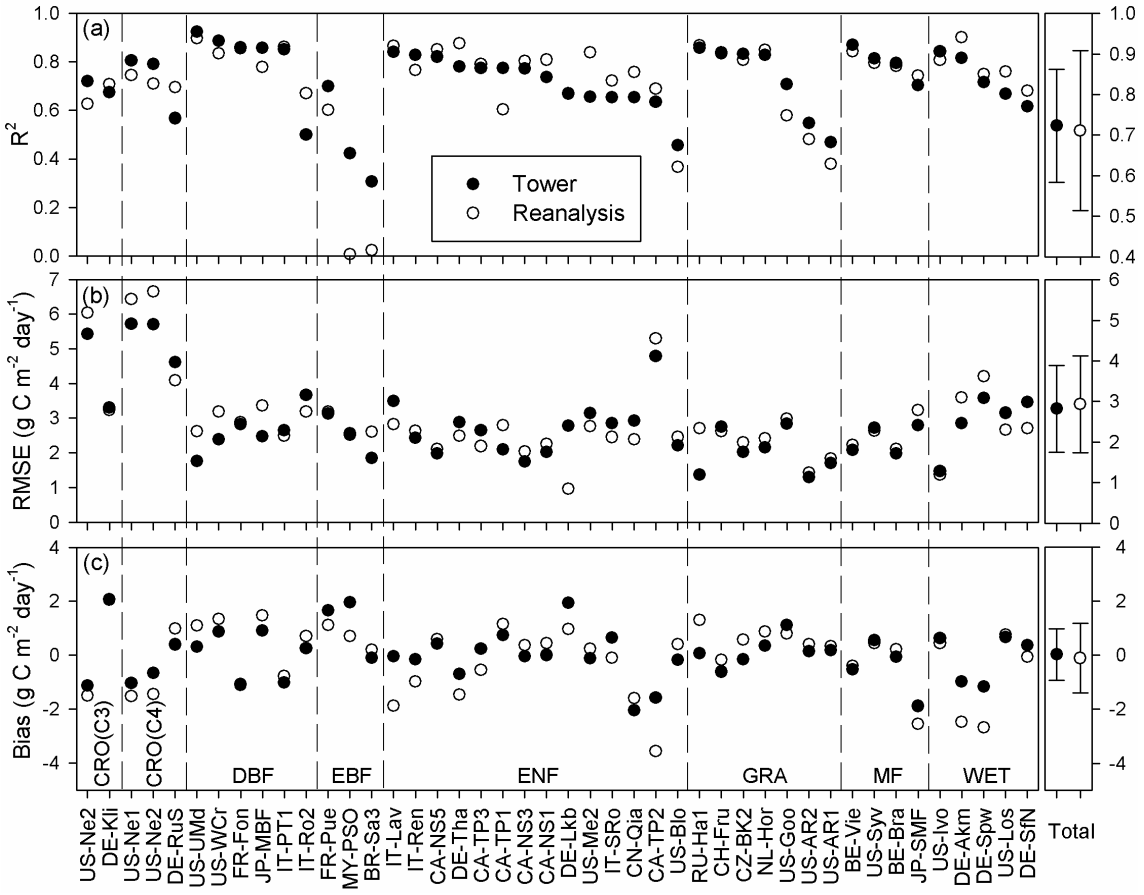


**Figure 3: Comparisons of 8-day mean GPP between the observations at 43 validation sites and the model simulations. Solid and open dots indicate the GPP simulations derived from tower-derived meteorology data and meteorological reanalysis dataset, respectively.**

https://doi.org/10.5194/essd-2019-126
Preprint. Discussion started: 7 August 2019


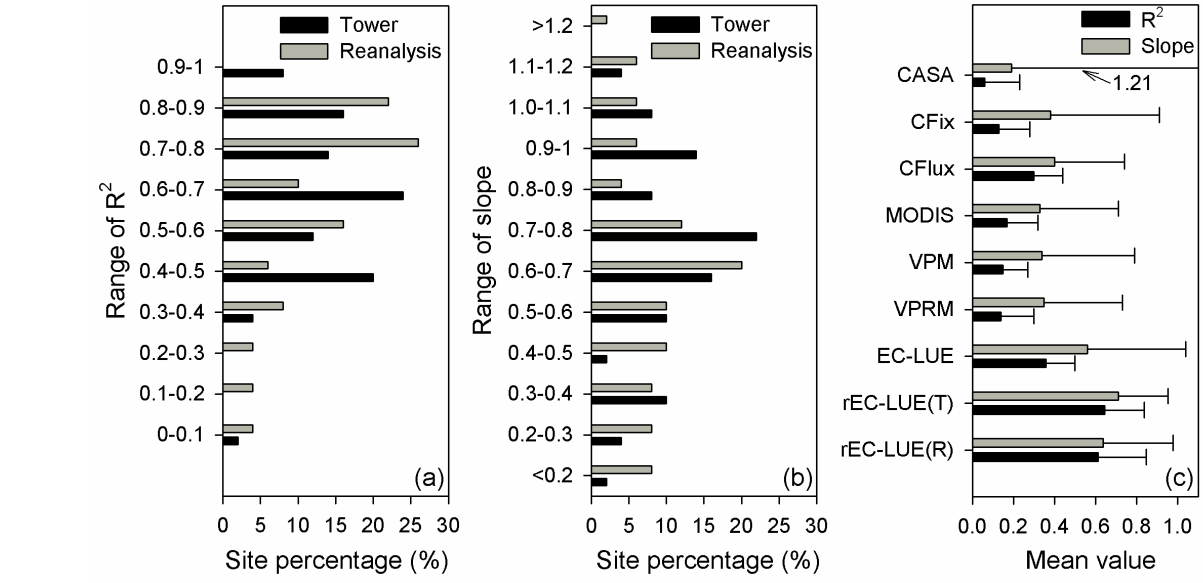


**Figure 4: Site percentage of (a) correlation coefficients ($R^2$), and (b) regression slopes between the model simulated and tower-based interannual variabilities in GPP. (c) Averaged values (error bars represent the standard deviations) of $R^2$ and slope for various LUE models. rEC-LUE (T) and rEC-LUE (R) indicate the revised EC-LUE models derived from tower-derived meteorology data and meteorological reanalysis dataset. The mean value of $R^2$ and slopes of the other seven LUE models in the figure were obtained from the study by Yuan et al. (2014).**

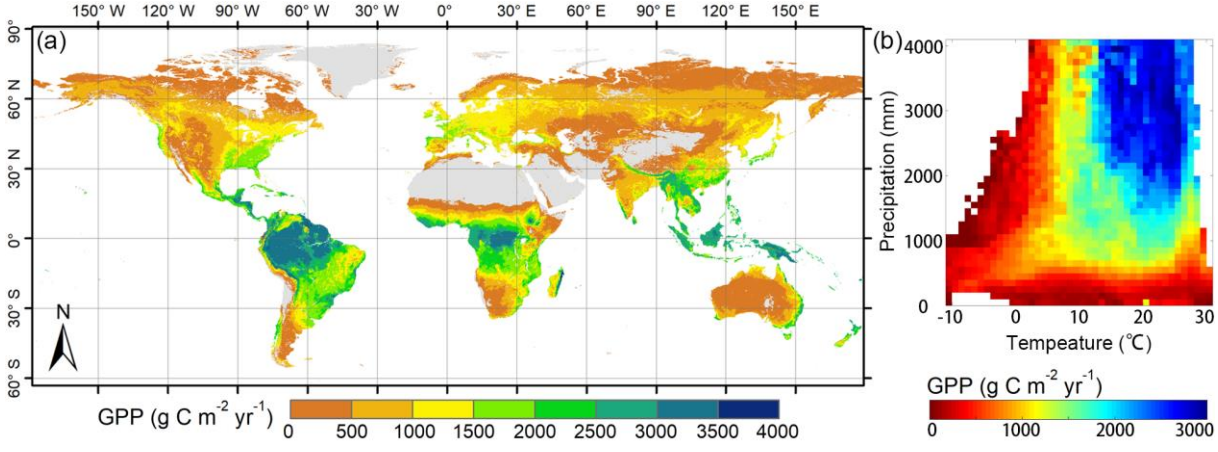


**Figure 5: Spatial pattern of global GPP simulated by the revised EC-LUE model during 1982–2017: (a) averaged annual GPP, (b) averaged annual GPP at different temperature and precipitation gradients.**

https://doi.org/10.5194/essd-2019-126
Preprint. Discussion started: 7 August 2019


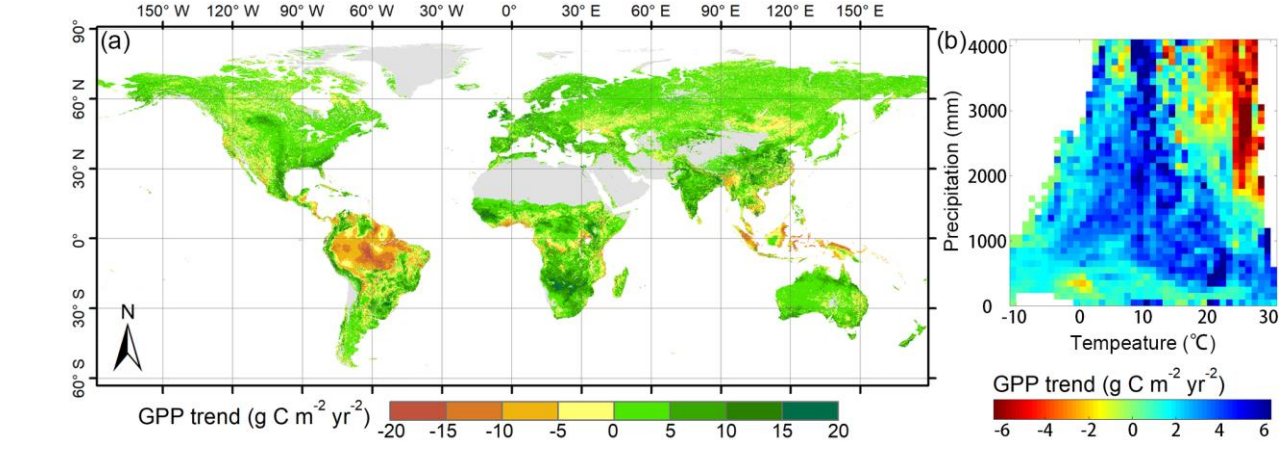


**Figure 6: Spatial pattern of global GPP trend simulated by the revised EC-LUE models during 1982–2017: (a) trend of annual GPP, (b) trend of annual GPP at different temperature and precipitation gradients.**

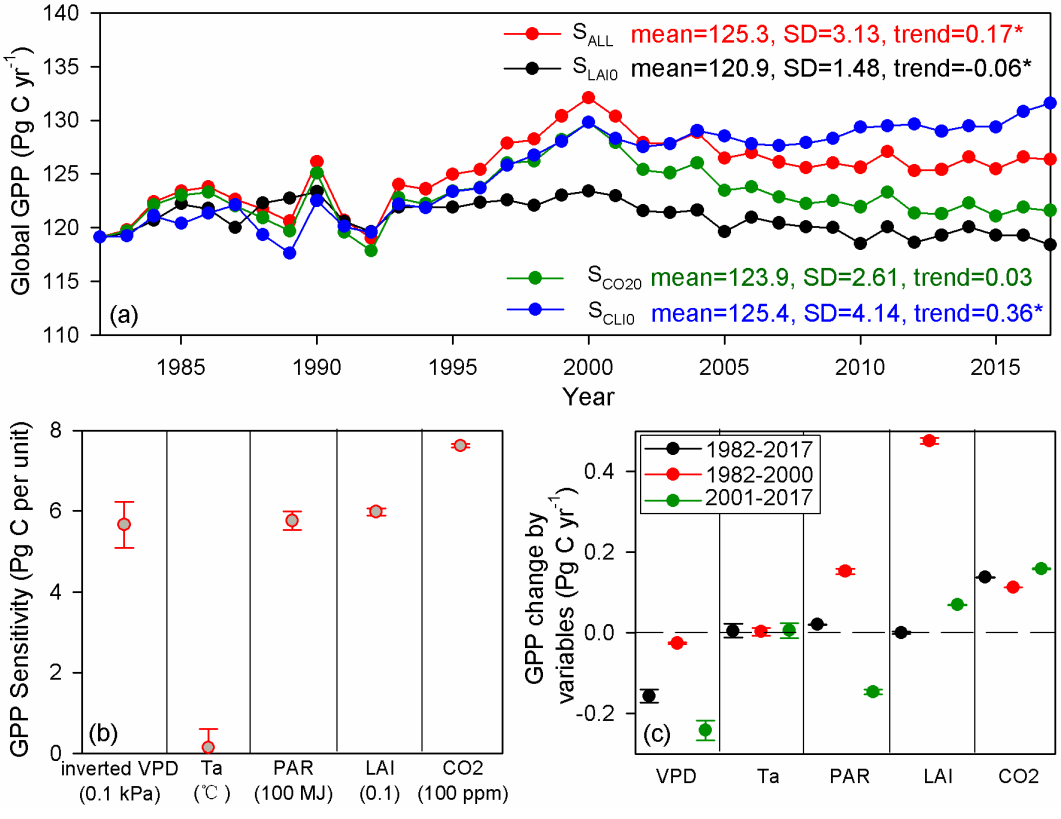


**Figure 7: Long-term changes in global GPP and the environmental regulations: (a) Global summed GPP derived from the four experimental simulations in section 2.4, (b) GPP sensitivity to climate variables (i.e., VPD, T, and PAR), LAI, and atmospheric $CO_2$, (c) contributions of climate variables (i.e., VPD, T, and PAR), LAI, and atmospheric $CO_2$ to GPP changes over 1982–2017, 1982–2000, and 2001–2017. * indicates the significant level at *p*-value<0.05.**

https://doi.org/10.5194/essd-2019-126
Preprint. Discussion started: 7 August 2019


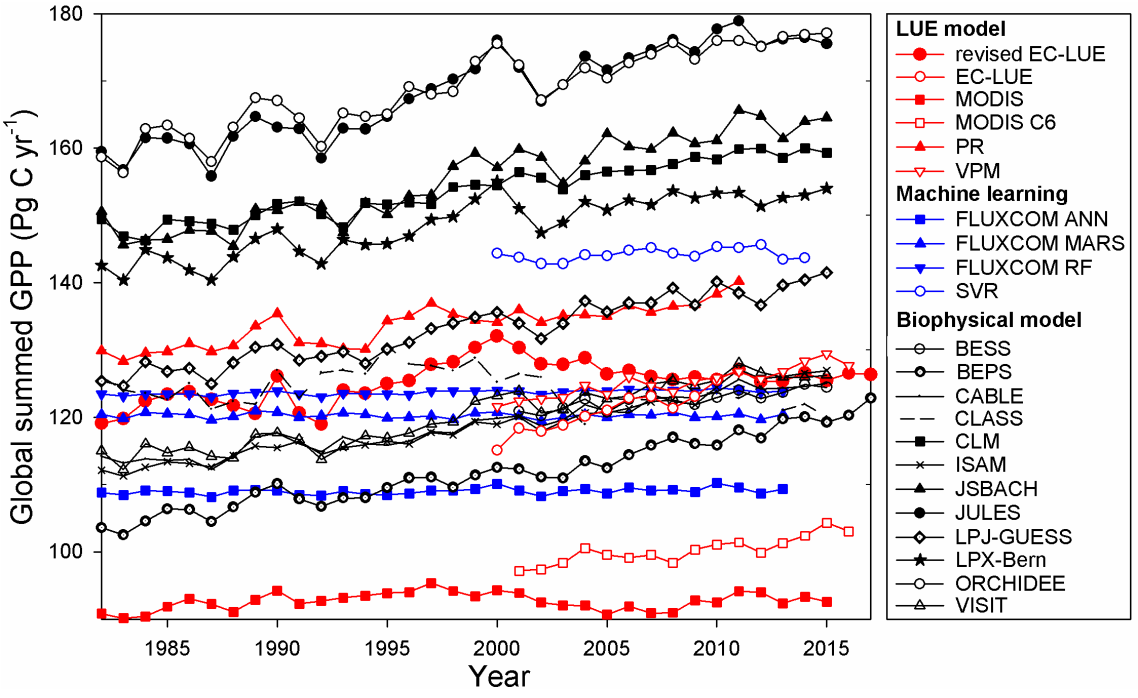


**Figure 8: Comparisons of annual global summed GPP estimates from various models. The datasets or model algorithms were obtained from: EC-LUE (Cai et al., 2014), MODIS (Smith et al., 2016), MOD17 C6 (Running et al., 2004), PR (Keenan et al., 2016), VPM (Zhang et al., 2017), FLUXCOM (Jung et al., 2017), SVR (Kondo et al., 2015), BESS (Jiang and Ryu, 2016), BEPS (Ju et al., 2006; Liu et al., 2018), and TRENDY. Ten of the twelve biophysical models (except BESS and BEPS) were the models in TRENDY.**

https://doi.org/10.5194/essd-2019-126
Preprint. Discussion started: 7 August 2019


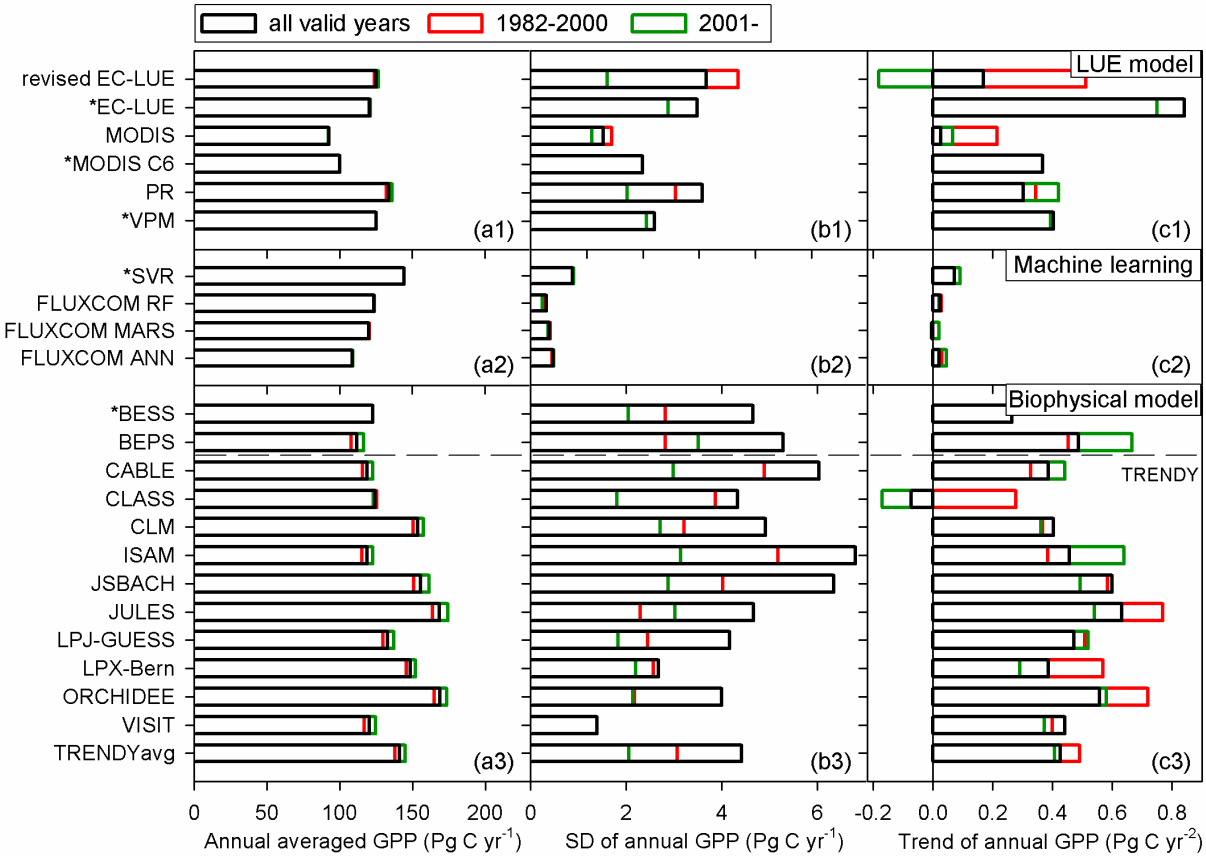


**Figure 9: Comparison of (a1)–(a3) averaged annual GPP, (b1)–(b3) interannual variability in annual GPP represented by standard deviation (SD), and (c1)–(c3) annual GPP trend among different GPP datasets or models. The references of these models are the same as in Figure 9. ∗ indicates that the valid period of the dataset is beginning from 2000 or 2001. TRENDYavg is the averaged GPP of the ten TRENDY models.**